

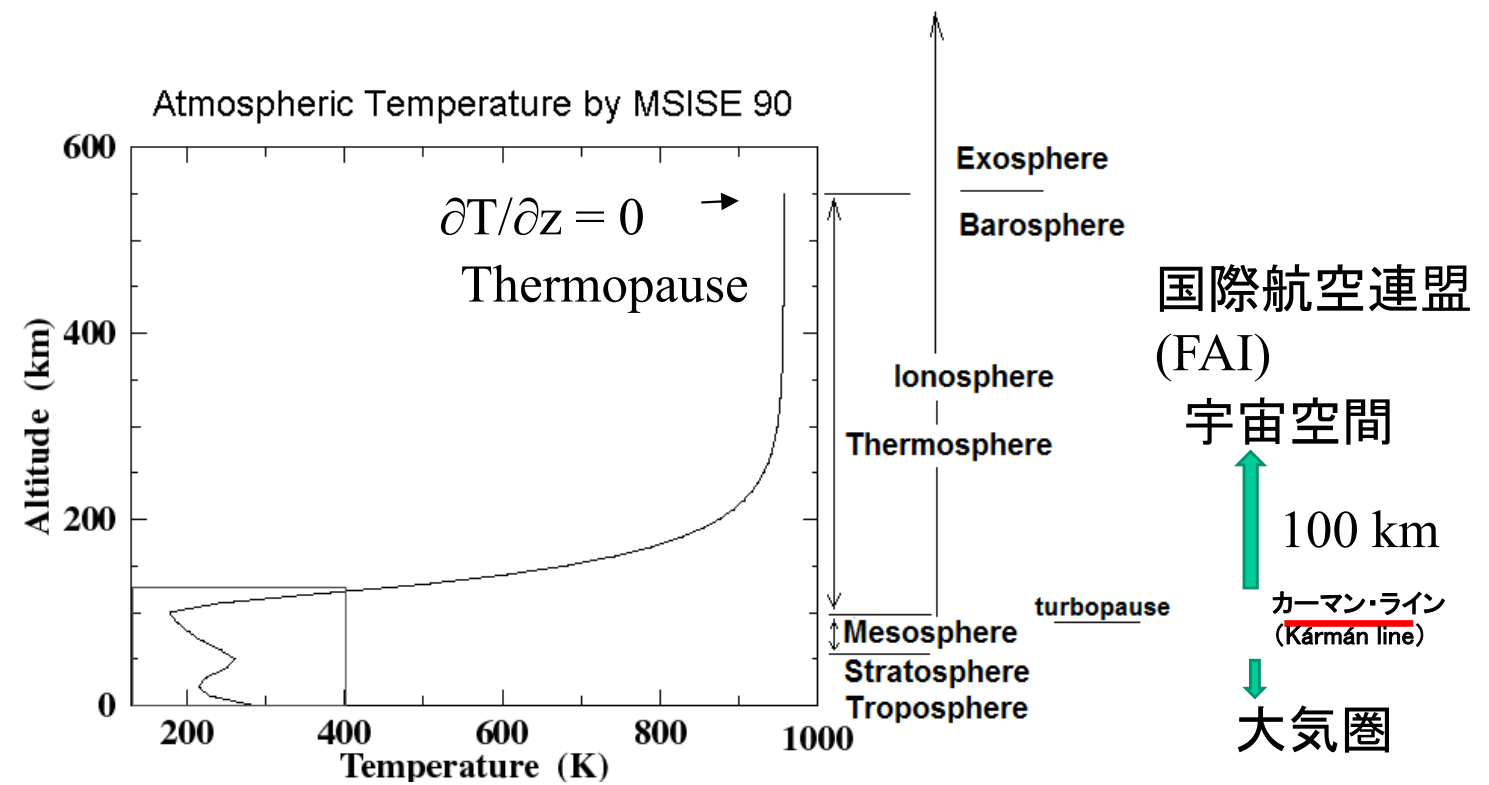
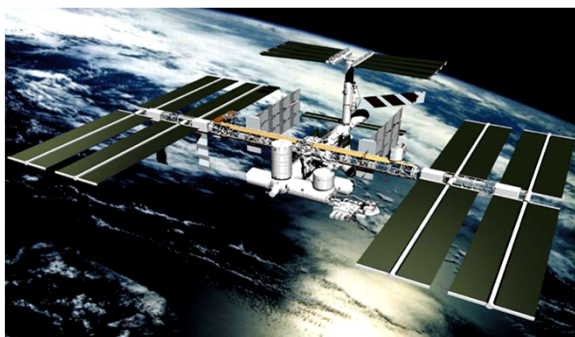


衛星・地上観測と コンピュータシミュレーション による超高層大気研究

成蹊大学

藤原 均

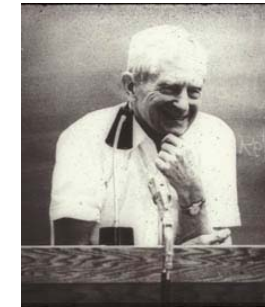
1. 熱圏について



Aeronomy

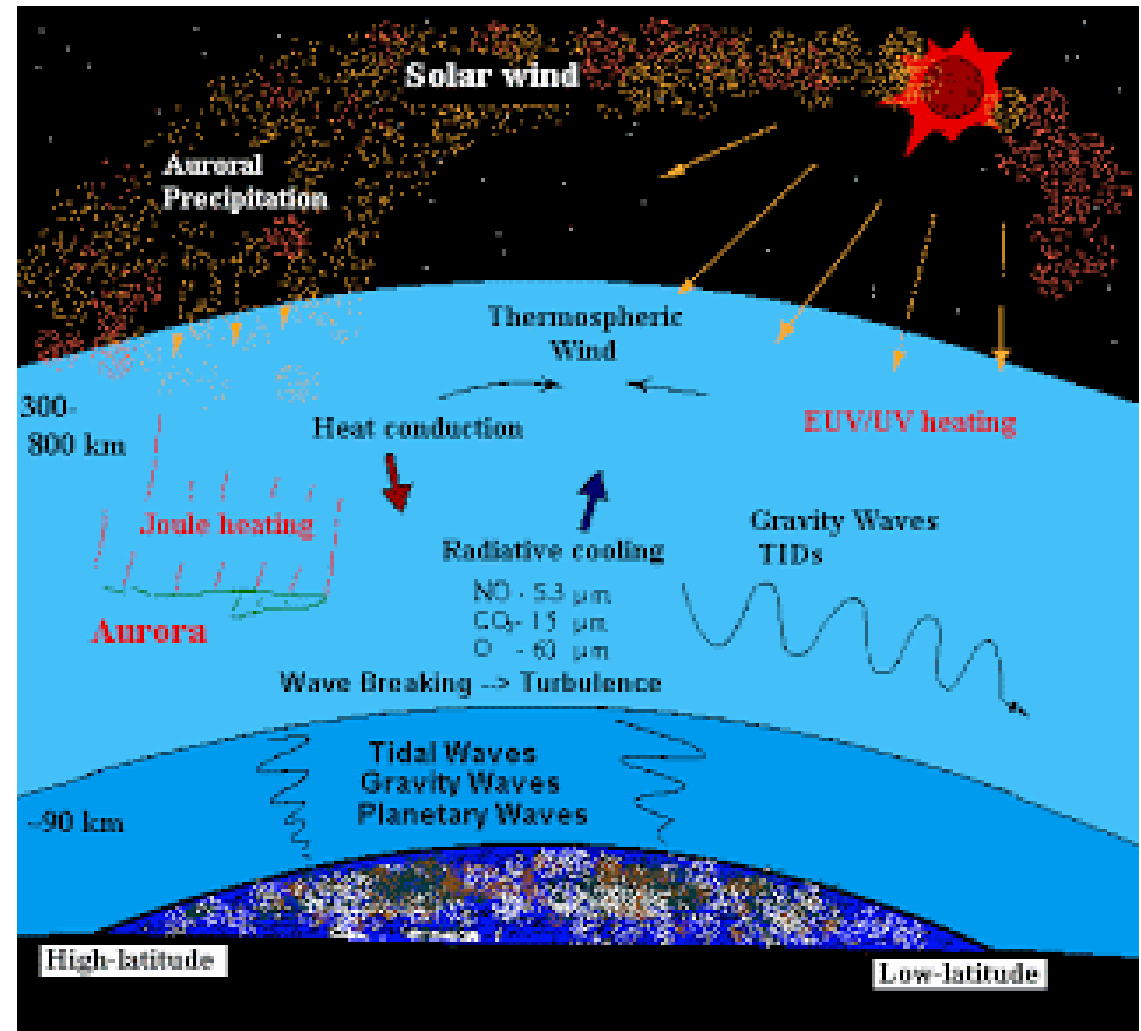
= Aero + nomy

The term aeronomy was introduced by Sydney Chapman in a Letter to the Editor of Nature (journal) entitled Some Thoughts on Nomenclature in 1946.

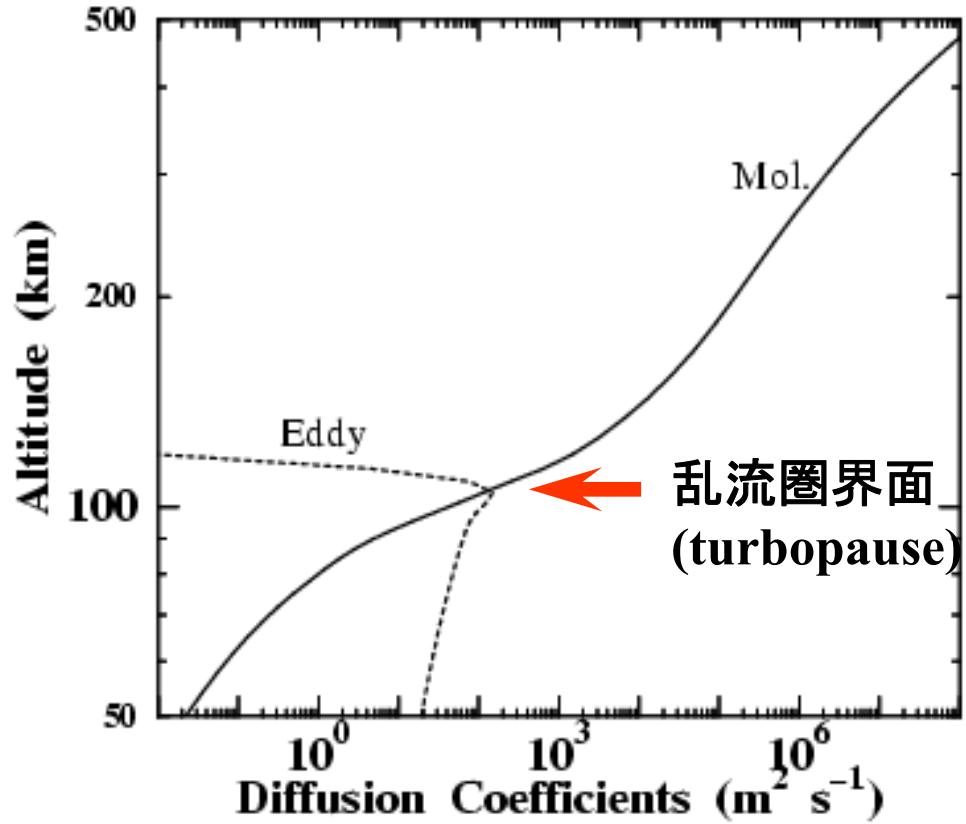


大気科学 天文学

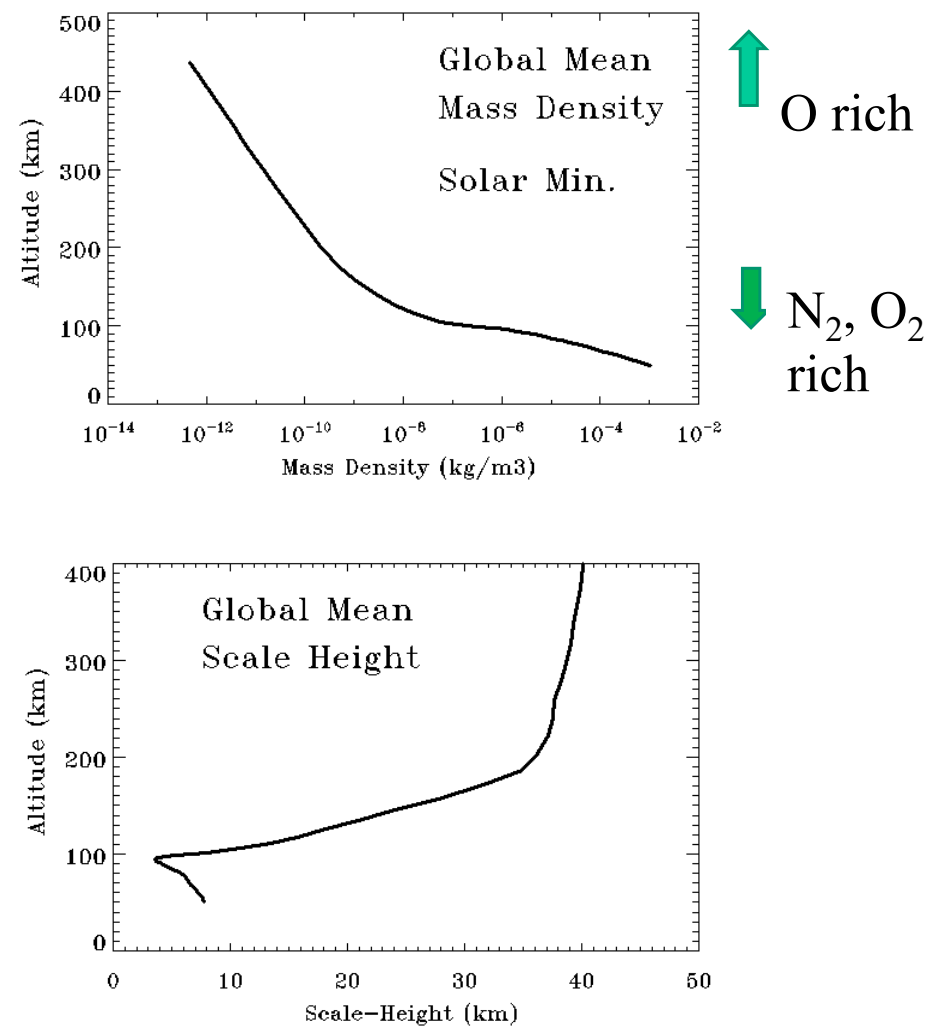
- ・流体的世界+粒子の世界
(熱圈界面: スケールハイト~平均自由行程)
- ・乱流から分子過程へ
- ・中性とプラズマが混在
- ・特殊な放射
 LTEからnon-LTEへ
- ・様々な大気波動
- ・磁気圏と下層大気からのエネルギー流入



(from 1D model calculation)

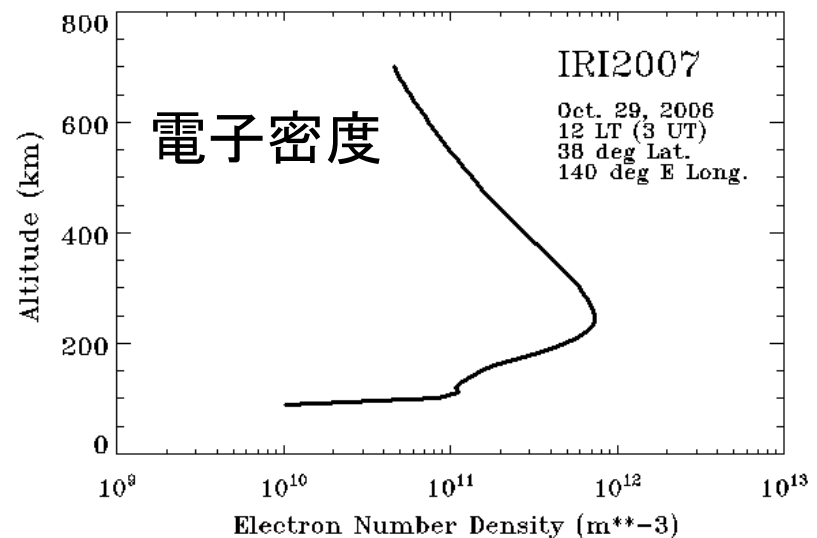
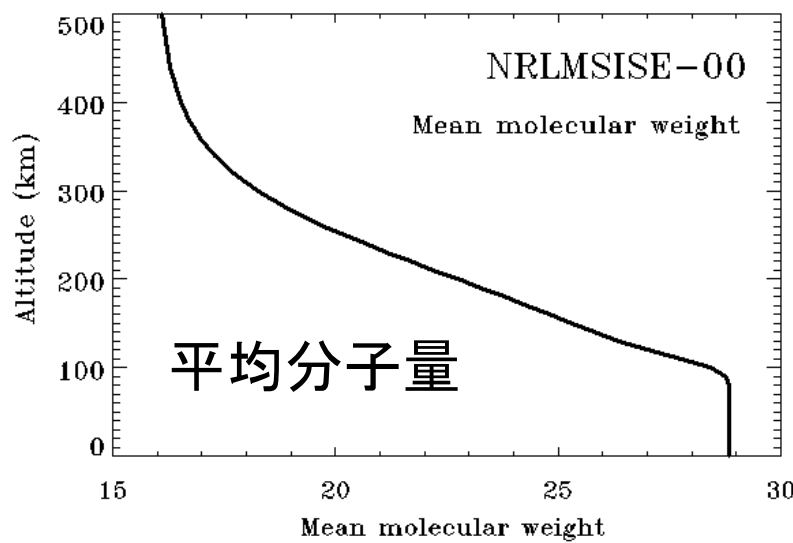
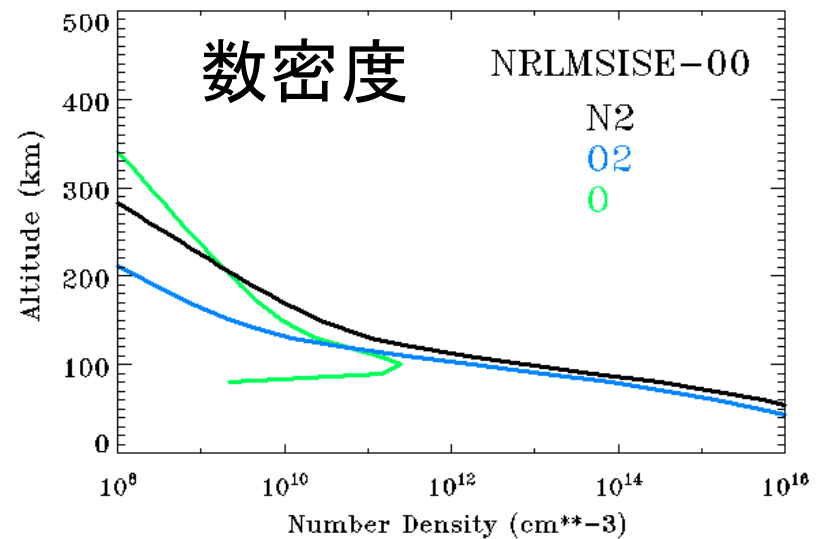
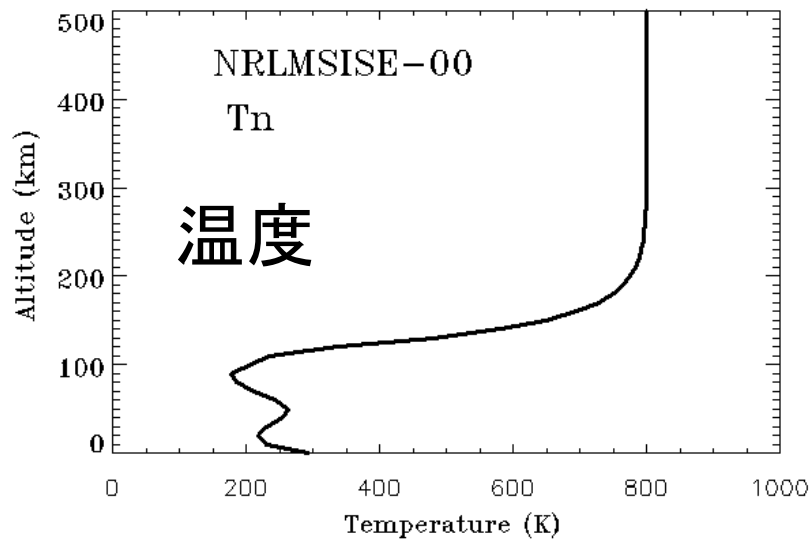


分子拡散(Mol)、渦拡散(Eddy)
係数の高度プロファイル。

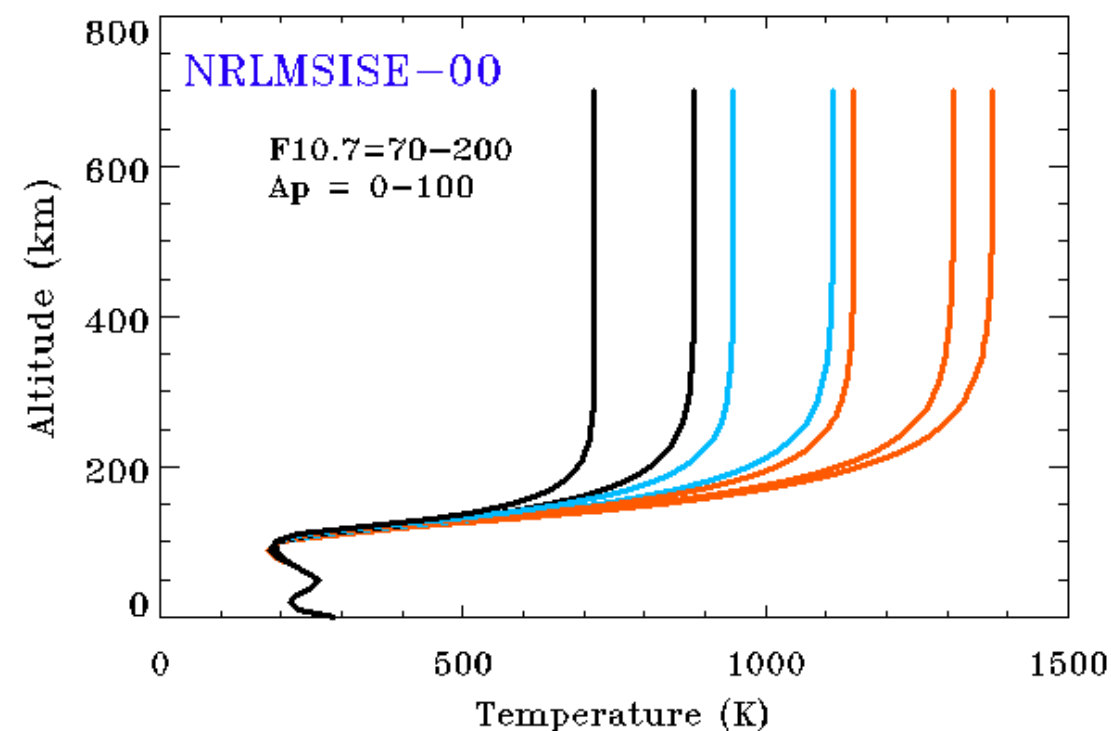
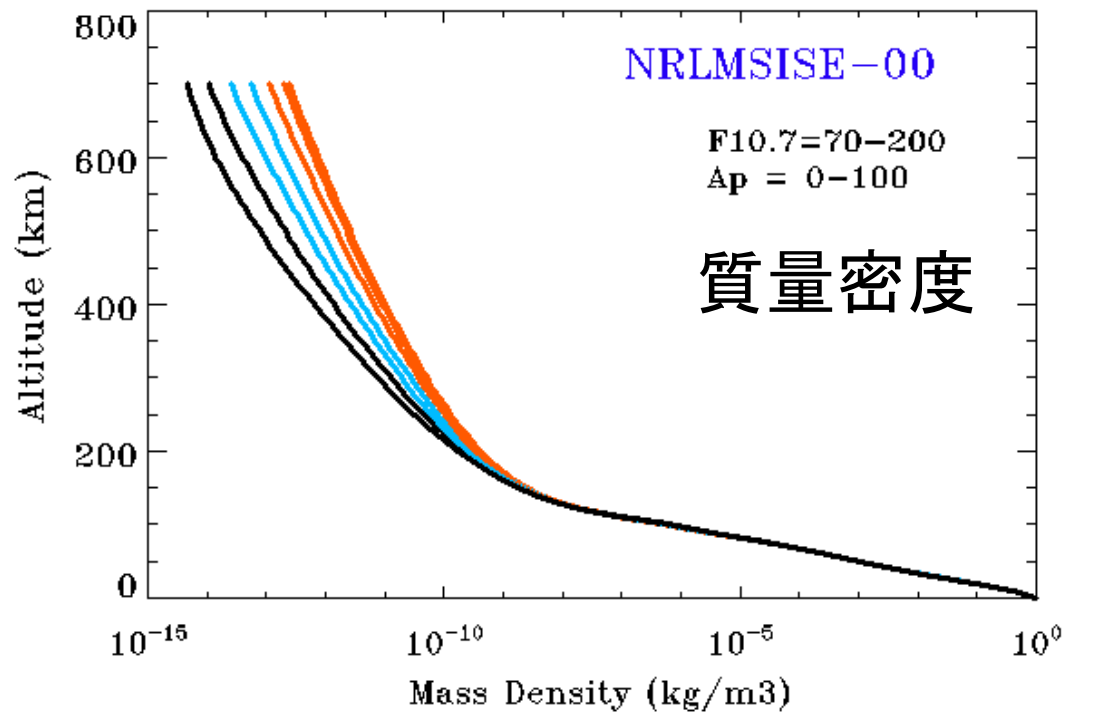


熱圏大気について

Thermosphere

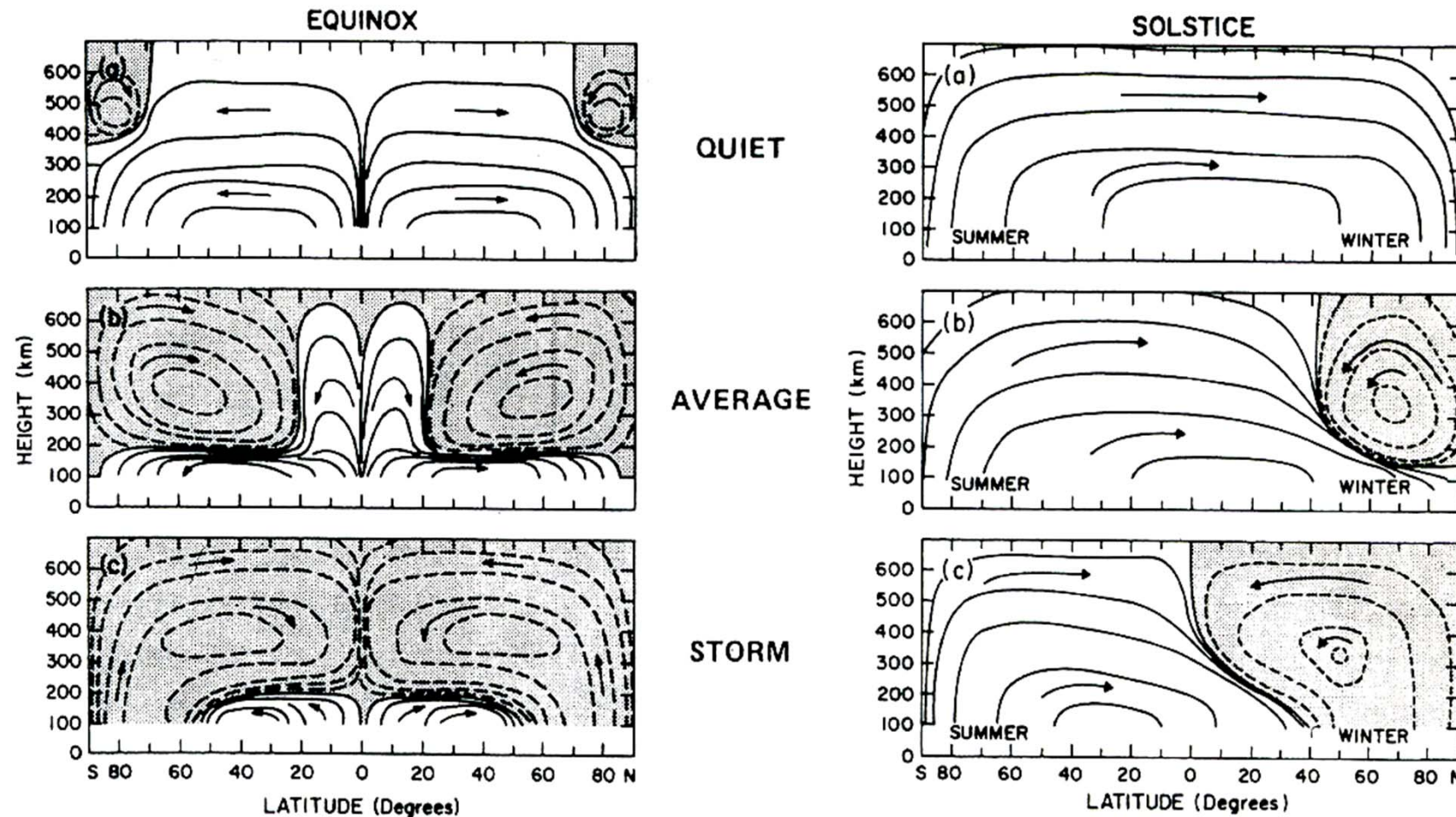


太陽活動や オーロラ活動 による変化



熱圏大気の子午面循環

子午面循環を2つの熱源が駆動する: 赤道…太陽紫外線加熱、
極域…オーロラ加熱



Roble (1987)

超高層大気の大循環

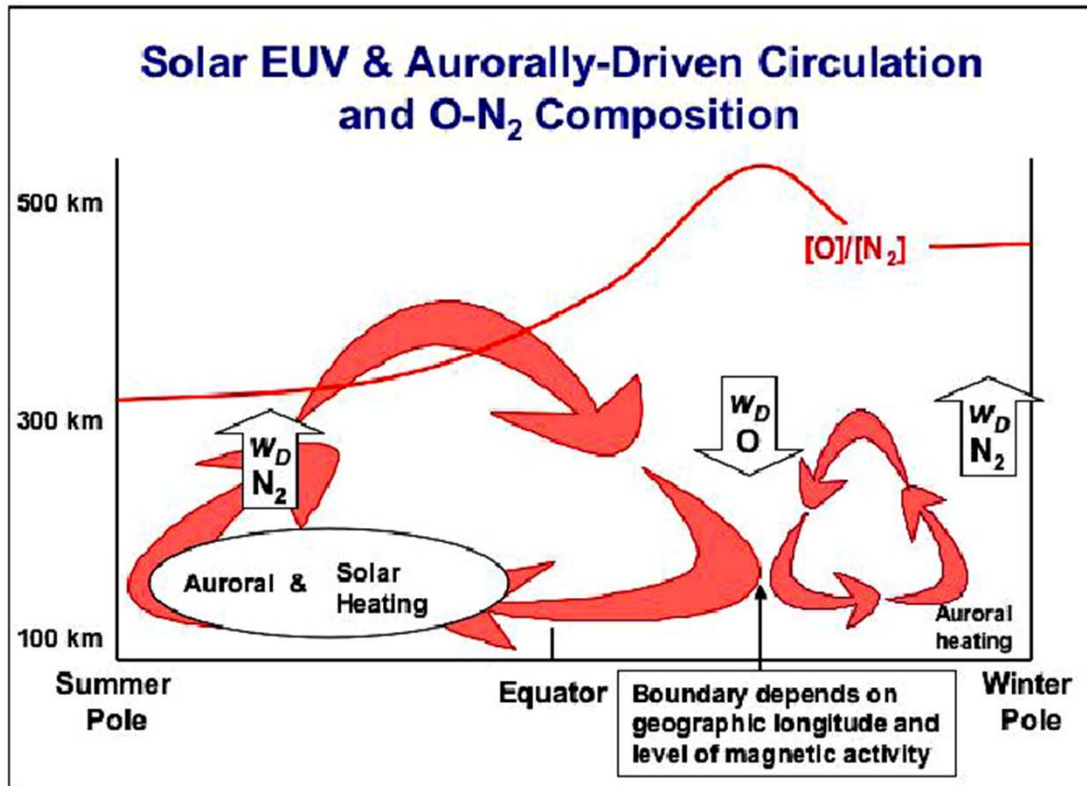
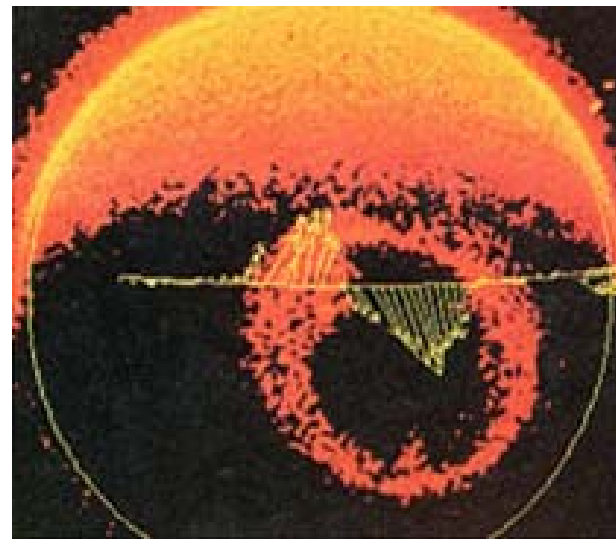


Figure 7. Same as Figure 6, with effects of high-latitude heating due to magnetospheric coupling processes.

Forbes (2007)
(Journal of Meteorological Society of Japan)

電離圏プラズマの存在下における 中性大気の運動

$$\frac{d\mathbf{U}}{dt} = -2\Omega \times \mathbf{U} + g - \frac{1}{\rho} \nabla P + \frac{1}{\rho} \nabla \cdot (\mu \nabla) \mathbf{U} - \underline{\nu_{ni}(\mathbf{U} - \mathbf{V})}$$
$$(-\nu_{ni}(\mathbf{U} - \mathbf{V}) = \frac{1}{\rho} \mathbf{J} \times \mathbf{B})$$



DE1衛星による紫外
オーロラ撮像とDE2
衛星による中性風観測

(Killeen et al., 1988)

2. 熱圏・電離圏モデルの開発史

英國(UCL+Shefield Univ, NOAA)と米国(NCAR)の開発競争

Fuller-Rowell et al. (1980)が熱圏大気大循環モデルの始まり。
Roble et al. (1981)が次いで発表される。

Fuller-Rowell et al. (1987)が熱圏・電離圏モデルの始まり。
Roble et al. (1988)が次いで発表される。



Timothy J. Fuller-Rowell

<https://cires.colorado.edu/council-fellows/timothy-j-fuller-rowell>



Raymond G. Roble

<https://www2.hao.ucar.edu/news/2014-jan/roble-honored-bowie-medal>

Fuller-Rowell et al. (1980) → ... → CTIM, CTIPe, IDEA
Roble et al. (1981) → ... → TIE-GCM, TIME-GCM,
WACCM-X

気象モデル → 熱圏モデル → 熱圏・電離圏モデル

→ 各種結合モデル

熱圏・電離圏・磁気圏結合モデル

全大気圏・電離圏結合モデル

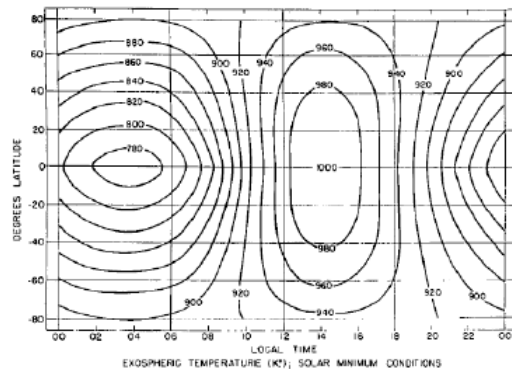
(WACCM-X, IDEA, GAIAの3つのみ)

→ 惑星超高層モデル(金星、火星、木星、土星、タイタン)

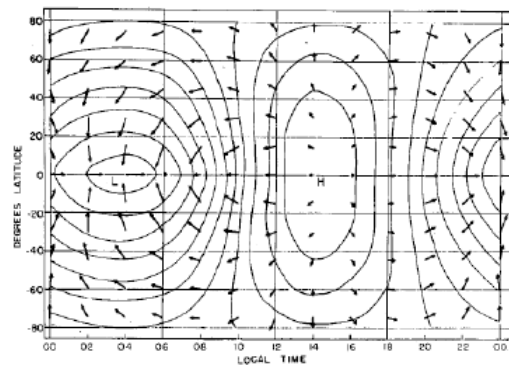
→ データ同化(NCAR, NOAAを中心に)

September 1968

R. E. Dickinson and J. E. Geisler



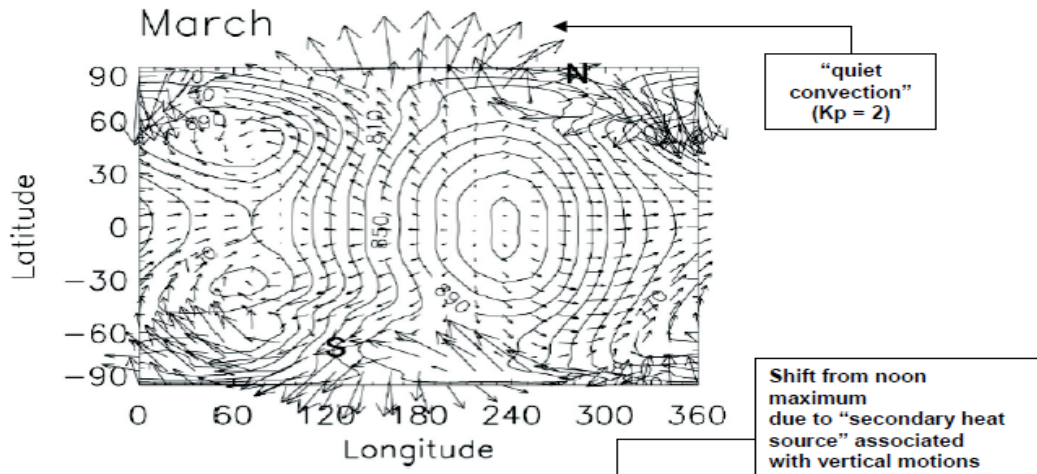
Exospheric Temperatures from Jacchia 1965 model, used with model densities to derive pressures and pressure gradients



Wind vectors calculated from momentum equation with Jacchia 1965 pressure gradient forcing. Isobars are shown by solid lines

CEDAR 2007 Student Workshop, June 2007

CTIP modeling (Rishbeth et al., 2000)



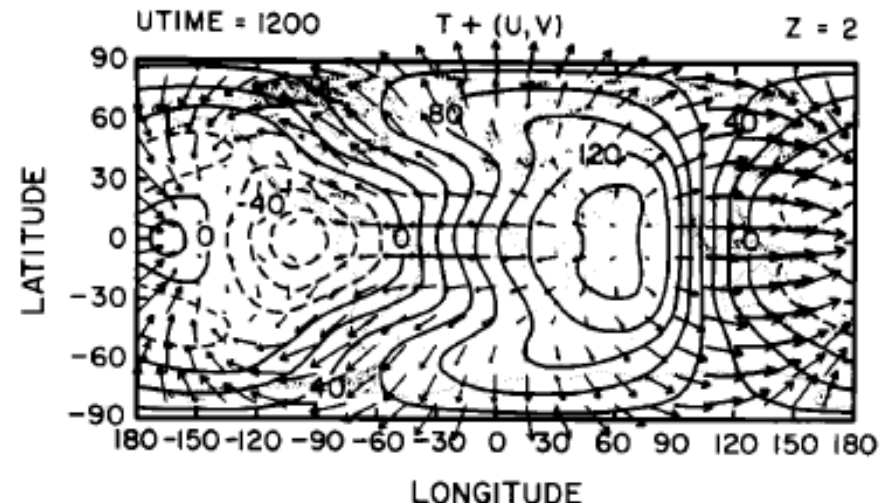
Exospheric temperatures peak near 15:30 h local time.

Day-night temperature differences at low latitudes reach around 200 K.

超高層の風は等圧線を横切って吹く。

下層の風は、等圧線に沿って吹く。(地衡風)

NCAR TGCM with tides



Perturbation temperatures from a constant global mean value (solid curves) and winds (arrows) at fixed pressure levels for Equinox conditions during solar minimum calculated by the TGCM with tides (Fesen et al., 1986)

超高層大気・電離圏モデルの種類

1. 統計(経験)モデル

NRLMSISE-00, NRLMSIS 2.0 (超高層物理学分野での標準モデル)

International Reference Ionosphere (IRI) (電離圏モデル)

DTM-2020, JB2008

Marshall Engineering Thermosphere Model (MET-2007)

2. 物理モデル

TIME-GCM, TIE-GCM, WACCAM-X (NCARモデル)

CTIM, CMAT, IDEA (NOAA, UCL)

Global Assimilation of Ionospheric Measurements (GAIM)

SAMI3(電離圏: NRL), AFRL Global Theoretical Ionospheric Model (GTIM)

Global Coupled Ionosphere Thermosphere-Electrodynamics Model

(Chinese model:GCITEM)

3. その他

AMIEなど (電場/ポテンシャル分布の導出)

The Global airglow model (GLOW)

Global Scale Wave Model (GSWM) : 大気波動(潮汐)モデル

Japanese model

Middle atmosphere
GCM

Based on a GCM by Japanese Meteorological Agency

Kyushu GCM (Miyahara,1991; Miyoshi,1999)

Miyoshi and Fujiwara (2003)
Whole atmosphere GCM

世界初の全大気圏モデル

Model inputs

potential data

EISCAT, MU,
EAR, PANSY,
IMAP, GPS,
SuperDARN,
FPI, Lidar, ...

Ground-to-topside model
of Atmosphere and
Ionosphere for
Aeronomy (**GAIA**)
(Jin et al., JGR, 2011)



Programs

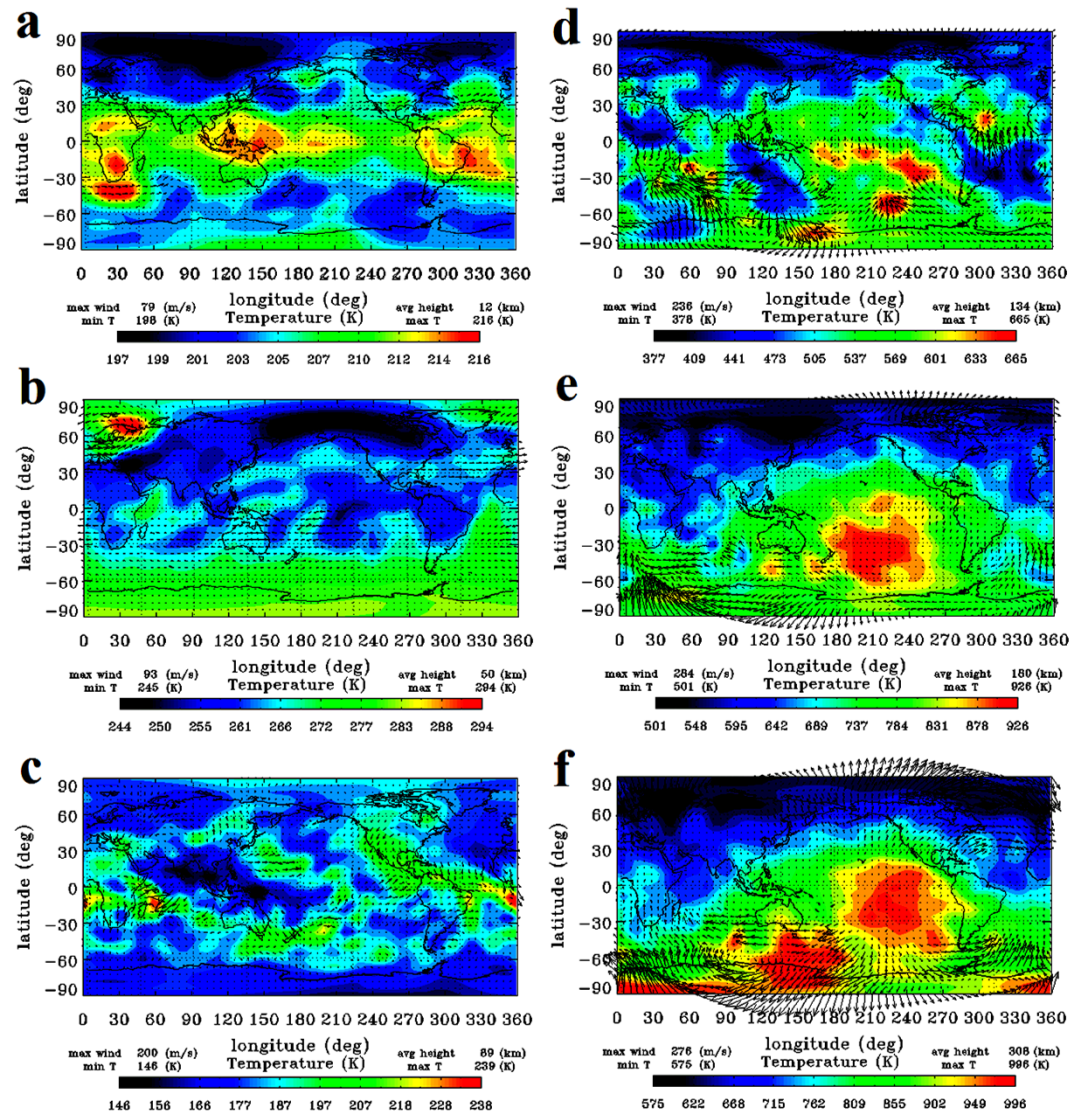
IMAP
Ground-based
observations
(EISCAT-3D)
FACTORS

2011
Kyushu Univ.
NICT
Seikei Univ.

3. 全大気圏モデル・ 大気圏-電離圏 モデル(GAIA)

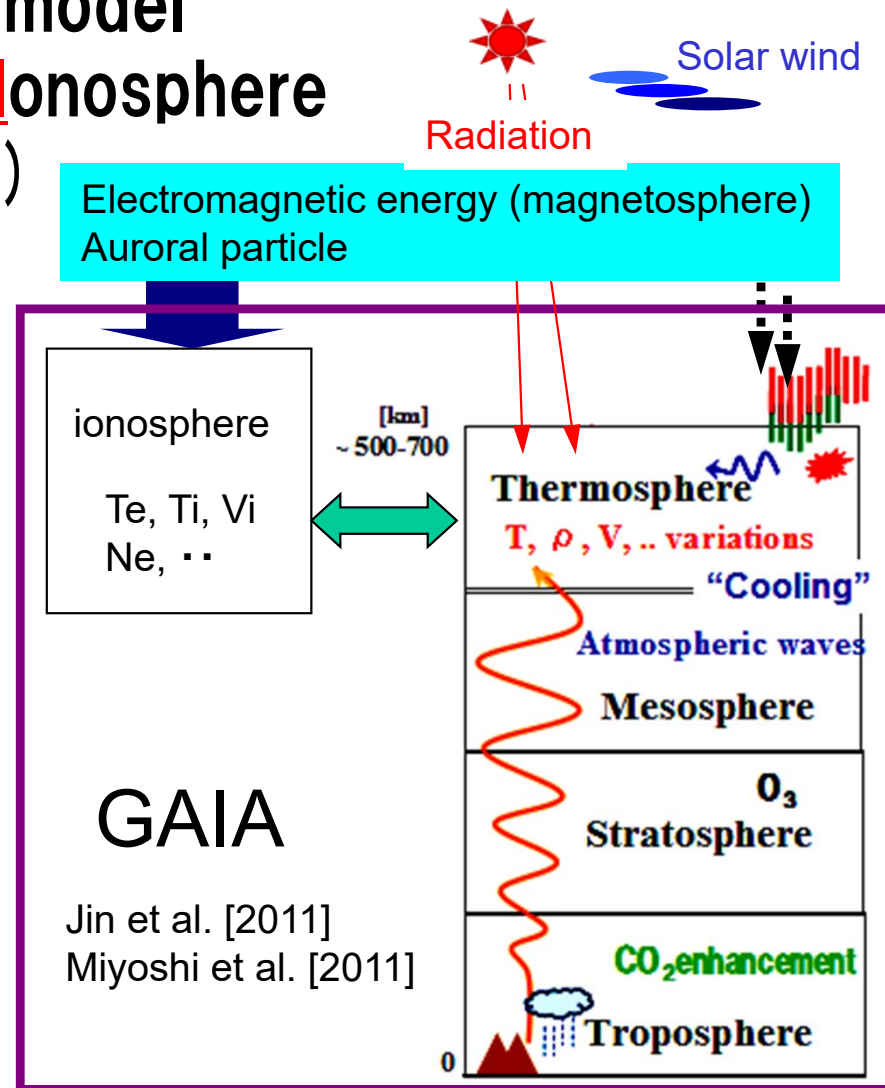
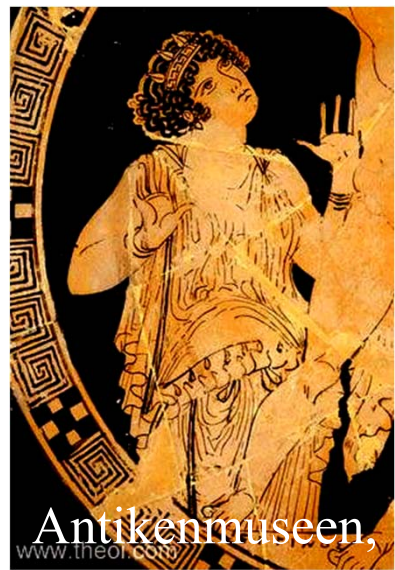
- a) 12 km
- b) 50 km
- c) 89 km
- d) 134 km
- e) 180 km
- f) 306 km

Solar min, Geomag quiet
(Fujiwara et al., 2011)

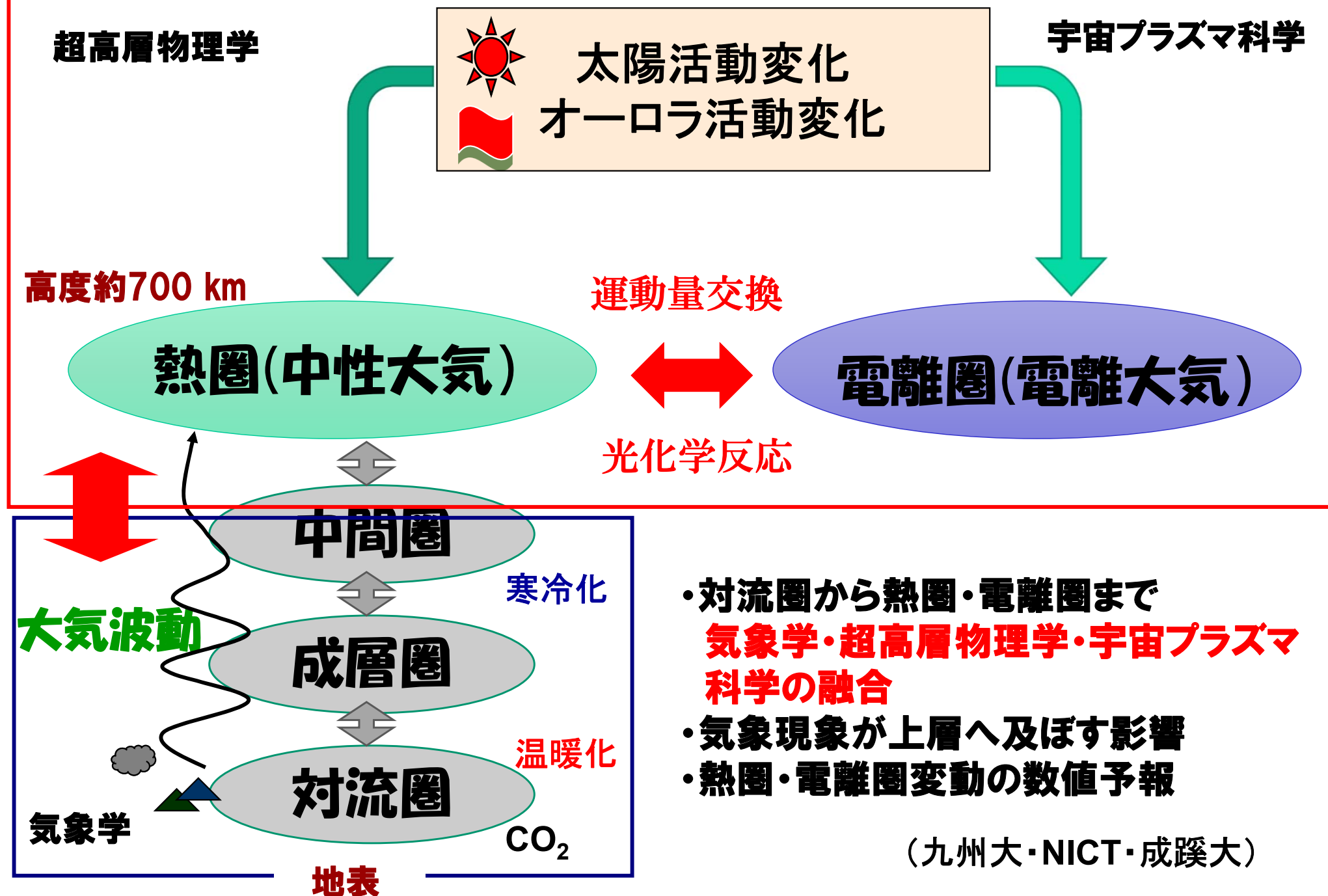


Ground-to-topside model of Atmosphere and Ionosphere for Aeronomy (GAIA)

*Gaia, the goddess
of the mother earth,
was born from chaos*



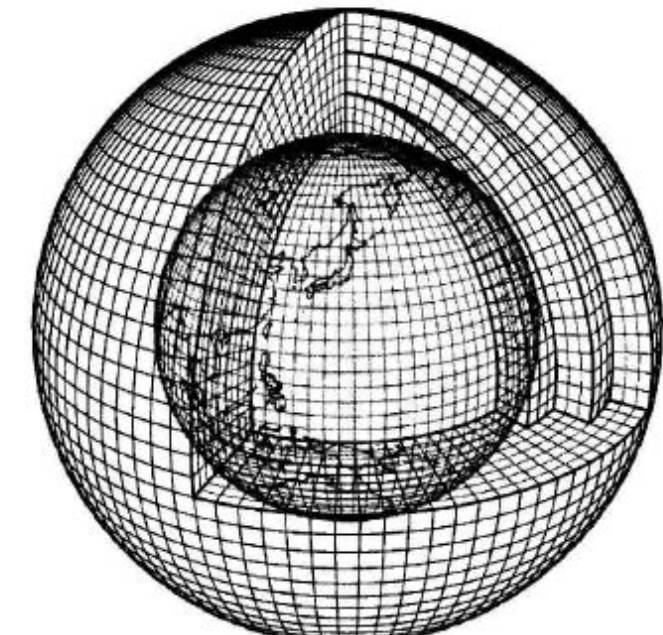
GAIA (Ground-to-topside model of Atmospheres and Ionosphere for Aeronomy)



数値モデル(GAIA)の概要

①中性大気を記述する大気大循環モデル

- ・気象の数値予報モデルを鉛直上方(熱圏上端まで)に拡張
- ・**全球**をいくつかの格子点に分割し、各格子点上で、物理法則(運動方程式、連続の式、熱力学の式、放射伝達の方程式など)を解き、**大気全層における風速、密度、温度、大気組成**などの3次元分布を計算・予測
- ・下層大気の観測値(海面水温、氷床、対流圏循環の状態)および太陽活動度や磁気圏からのエネルギー降り込み量を基に、全大気の状態を物理的に計算



②電離大気を記述する電離圏モデル

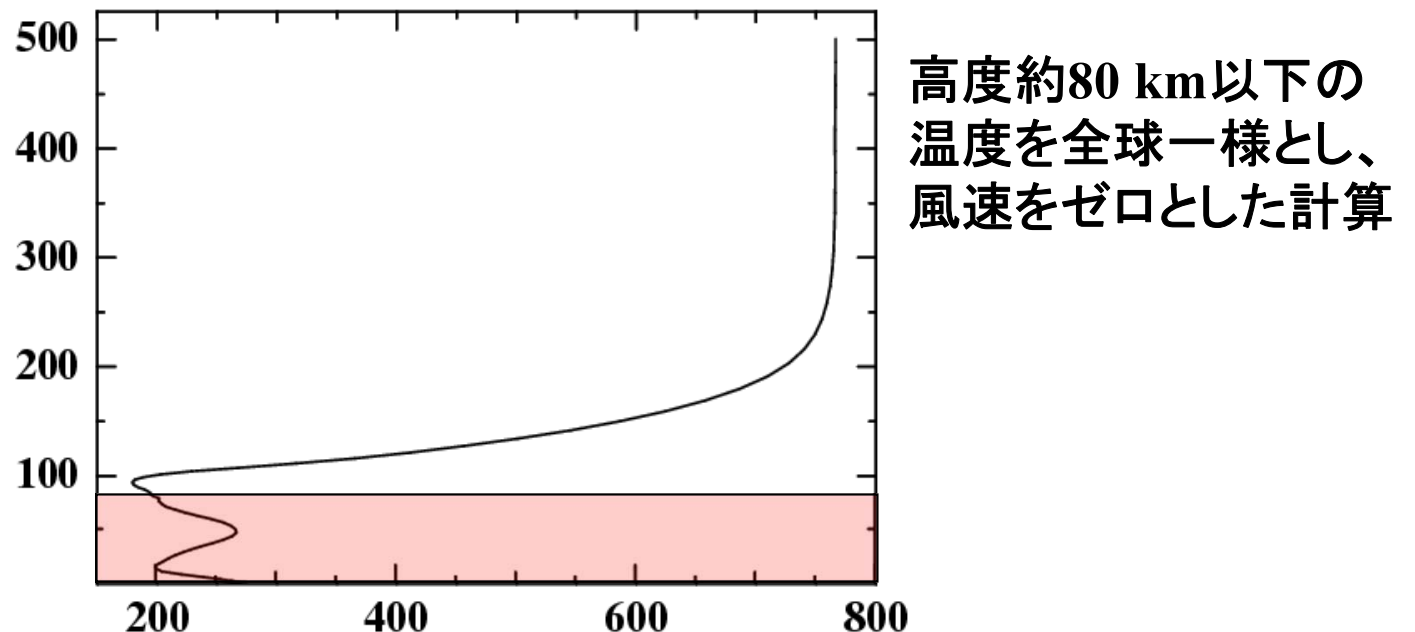
③電気力学過程を記述するダイナモモデル

数値モデル(GAIA)の特徴

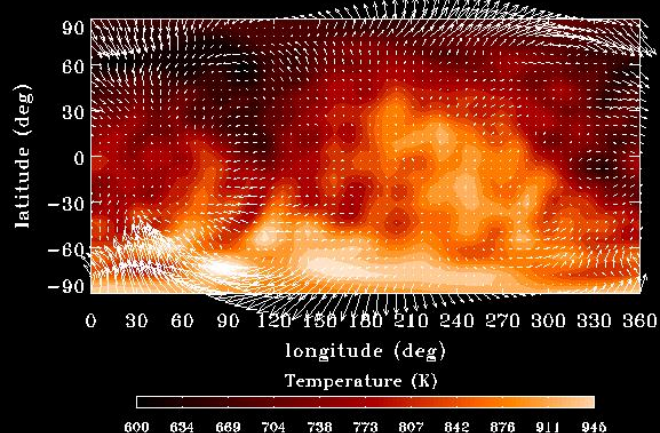
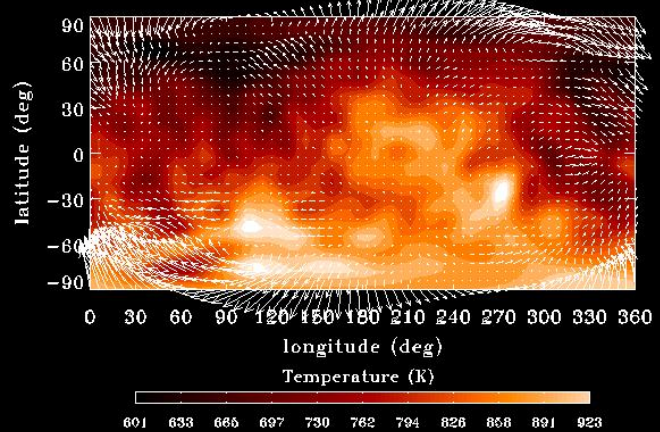
	数値モデル(GAIA model)	統計モデル(<i>e.g.</i> MSIS model)
長所	<ul style="list-style-type: none">・数10分～数時間・数日の大気変動を再現可能・局所的な大気構造を表現可能・現象の物理機構を調査可能・全球を均等にカバーするデータが得られる	<ul style="list-style-type: none">・取り扱いが比較的簡単(PCで動作可能。様々なプログラムへの組み込みが可能)・平均的な大気構造を容易に表現・理解できる
短所	<ul style="list-style-type: none">・高時間・空間分解能にするほど高度な計算機資源(スーパーコンピュータ)が必要・物理・化学過程のモデル化に際し、仮定が必要・非線形方程式を数値的に解いていることから、何らかの観測との比較が必要(適用限界の把握が難しい)	<ul style="list-style-type: none">・その時々の大気の状態をうまく表現できない・局所的な大気構造を表現できない・変動の時間変化をうまく表現できない

熱圏の局所構造は、下層大気の影響と考えられる。

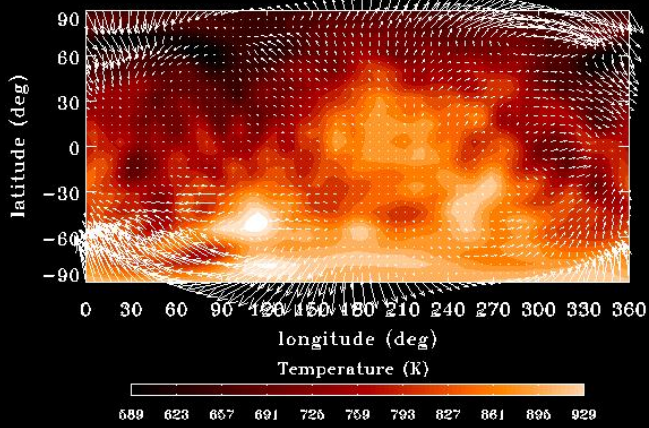
→ 下層大気が上層に及ぼす影響はどのくらいか？
下層大気変動あり・なしの数値実験



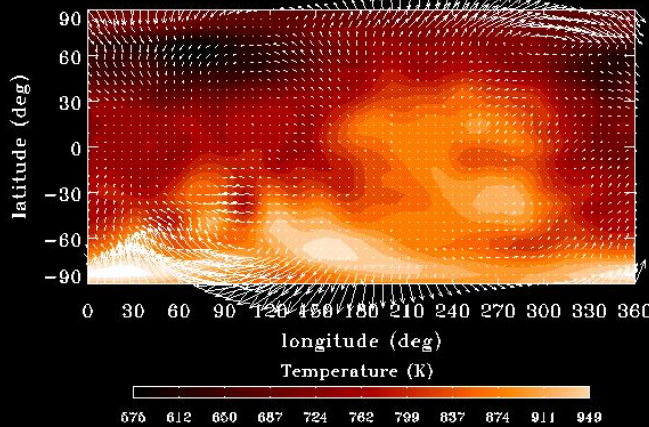
Results for usual calculations (about 306 km alt. UT=1)



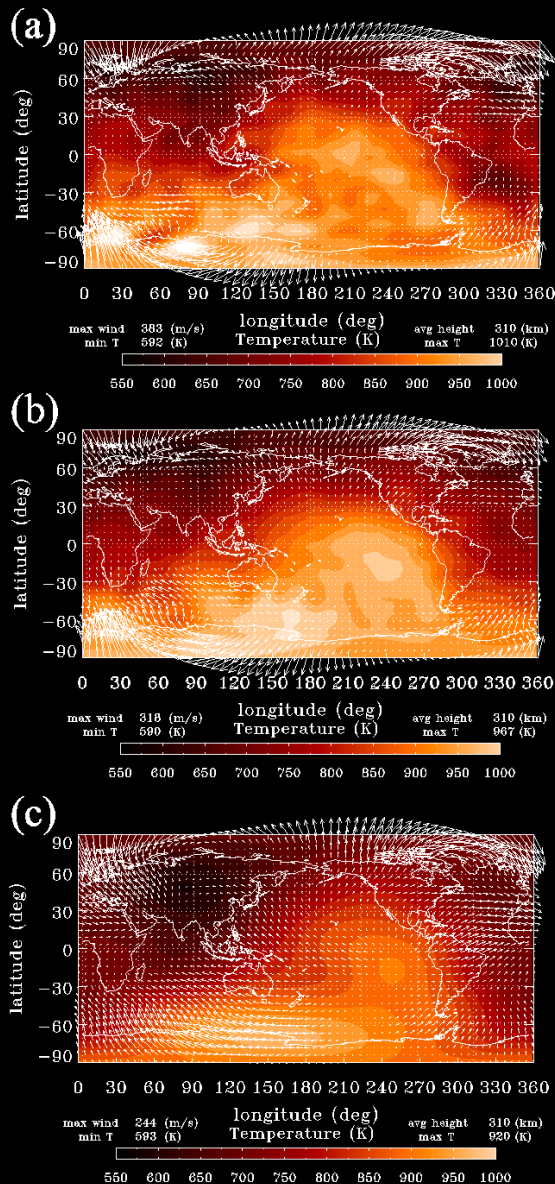
Suppression of effects from the lower atmosphere



After
1h



After
1day



上から、

(a) 通常の計算

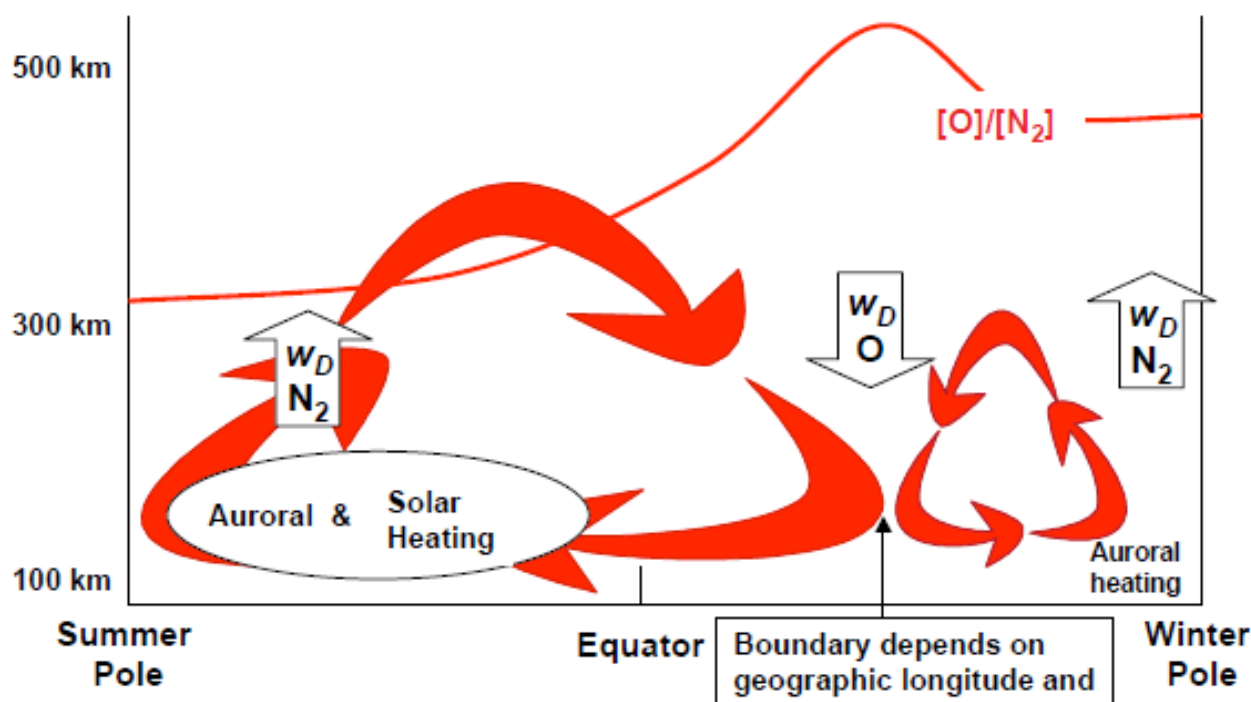
(b) 5日間の平均

(c) 経験モデル(NRLMSIS-00、HWM93)

The global distributions of temperature and horizontal wind obtained from (a) GCM calculations on a constant-pressure surface (~ 310 km altitude) at 01:00 UT on December 1, (b) 5-day average of GCM calculations at 01:00 UT, and (c) the NRLMSISE-00 and HWM-93 empirical models. Note that the strength of the maximum wind vector is different in each

O/N₂のグローバル分布 ～ 大気循環とTAD/TIDの指標として

Solar EUV & Aurorally-Driven Circulation and O-N₂ Composition

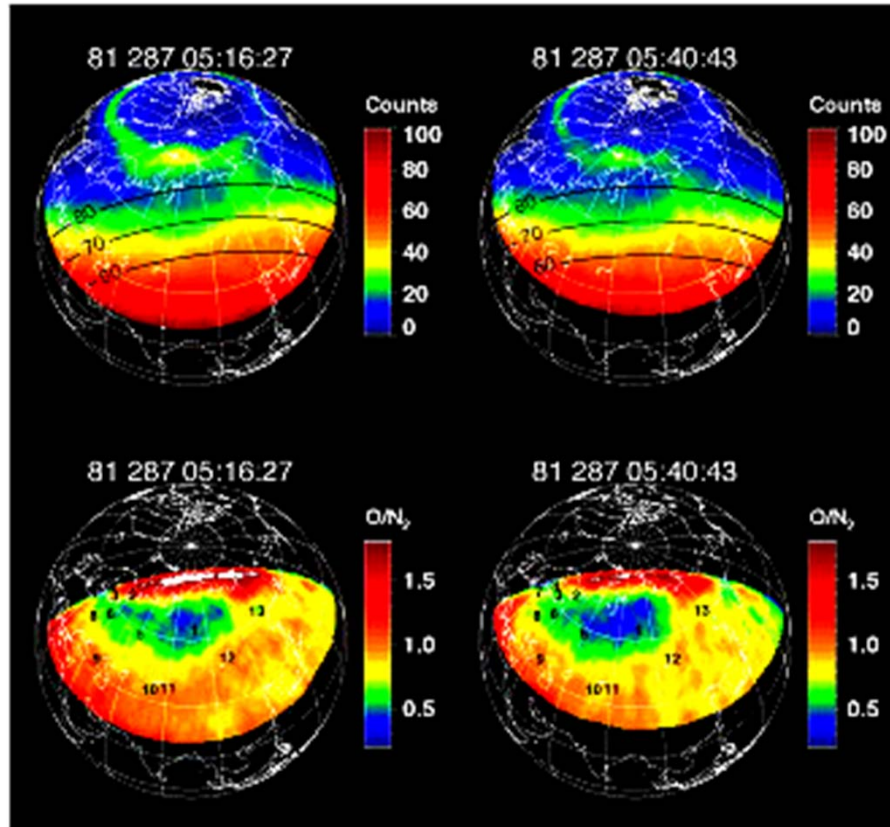


A secondary circulation cell exists in the winter hemisphere due to upwelling driven by aurora heating. The related O/N₂ variations play an important role in determining annual/semiannual variations of the thermosphere & ionosphere.

O/N₂の緯度、経度分布
日々変動、季節変動
太陽活動変化…
の詳細を知りたい。

- ↓
・大気循環の変化が議論できる
- ・昼側電子密度が推定可能
- ・磁気嵐時の伝搬性擾乱の時空間変化がわかる

O/N₂データとして、
AE衛星などに搭載された
質量分析器によるもの
がほとんどだった。

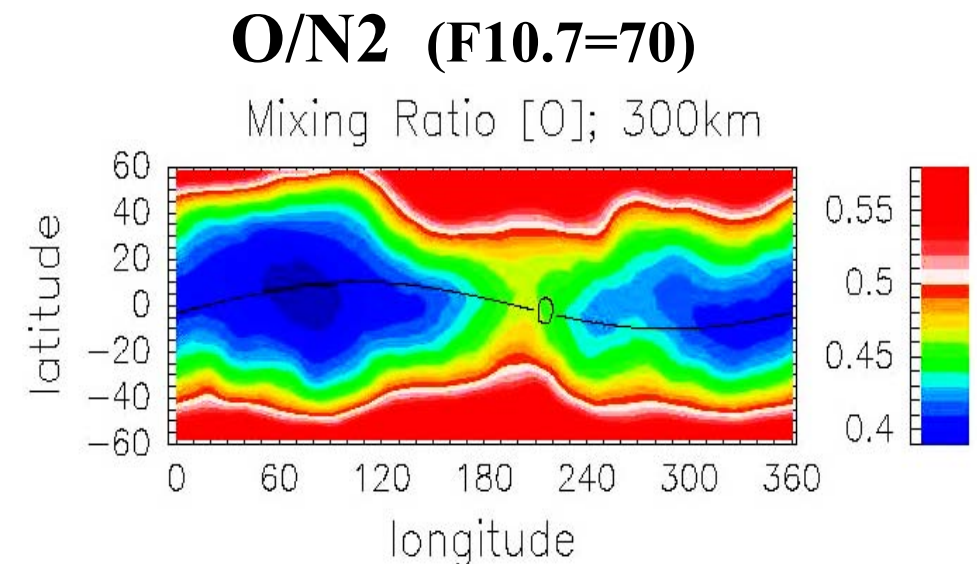
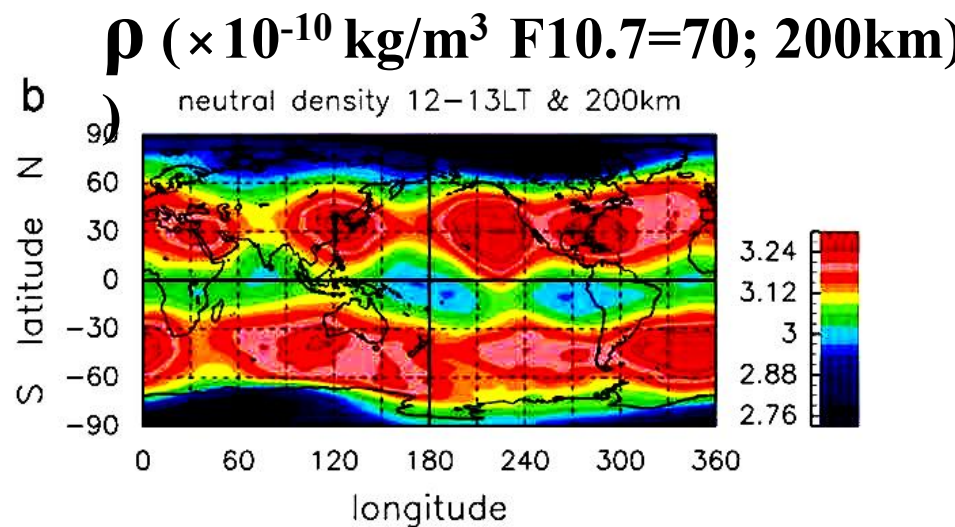


広範なO/N₂分布を得る手段として、紫外観測データを用いる方法がStrickland et al.(1995)によって提案された。
DE1のFUV観測の例
上図がカウント値で、下図がO/N₂を導出したもの。

DE1で個々の事例が示された。

定常観測出来れば、データ同化に利用可能？

GAIAによる計算例 11-12 LT



航空宇宙分野では、原子状酸素の情報が重要



(写真提供: JAXA)

下部熱圏での酸素原子密度推定例

- 63μm放射、balloon platform at 37 km

10ヶ月間低軌道にあって1996年1月に回収された無人宇宙実験システム・SFUの電気推進実験表面に取り付けられたポリイミド熱保護膜の回収後の姿。

JOURNAL OF GEOPHYSICAL RESEARCH, VOL. 92, NO. D4, PAGES 4325–4336, APRIL 20, 1987

Atomic Oxygen in the Lower Thermosphere

FLORENCE J. LIN, KELLY V. CHANCE, AND WESLEY A. TRAUB

Harvard-Smithsonian Center for Astrophysics, Cambridge, Massachusetts

We measured in thermal emission the 63- μm line due to thermospheric atomic oxygen $\text{O}({}^3P)$, using a far-infrared spectrometer on a balloon platform at 37 km altitude over Palestine, Texas (32°N), on June 20, 1983. From measurements of the equivalent width of this line at two elevation angles, we find a weak angular dependence: the equivalent width increases by a factor of 1.5 ± 0.3 as the angle decreases from $+30^\circ$ to $+1^\circ$. Since the optical depth of the $\text{O}({}^3P)$ line is large, we cannot directly convert the measured line intensity to a column abundance. Instead, we interpret the measurements in terms of radiative transfer through a 16-layer atmosphere extending to 200 km. We use a model atmosphere for summer at 30°N , with an exospheric temperature of 1300 K, including (1) an assumed daytime atomic oxygen abundance profile constructed from recent chemical and dynamical models and (2) a water vapor abundance profile constructed from recent experimental and model results. For this assumed $\text{O}({}^3P)$ vertical profile shape we determine from our spectra at two elevation angles a multiplicative scaling factor of 0.8, with an altitude-dependent uncertainty. In the best-determined layer the uncertainty in the multiplier is ± 0.2 at 119 km. The model-dependent peak atomic oxygen density is $3.6 (\pm 1.9) \times 10^{11} \text{ cm}^{-3}$ at an altitude of about 101 km.

A global measurement of lower thermosphere atomic oxygen densities

K. U. Grossmann, M. Kaufmann, and E. Gerstner

Department of Physics, University of Wuppertal, Wuppertal, Germany

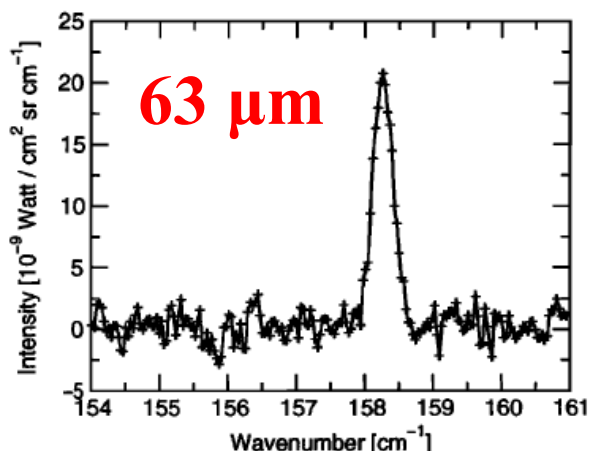


Figure 1. Single spectrum of the $O(^3P)$ emission line at $63 \mu m$ recorded by CRISTA-2 at an altitude of 151 km.

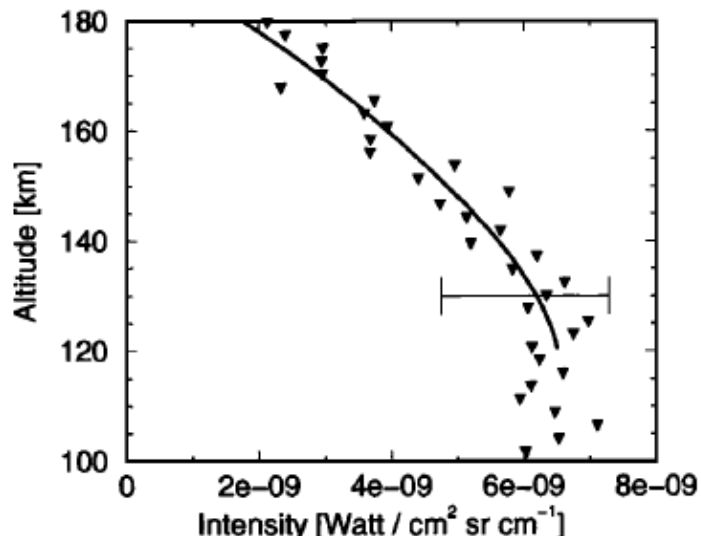


Figure 2. Line integrated limb radiance profile (CRISTA-2, one altitude scan). For details see text.

1994, 1997にスペース
シャトルから放出

140 km

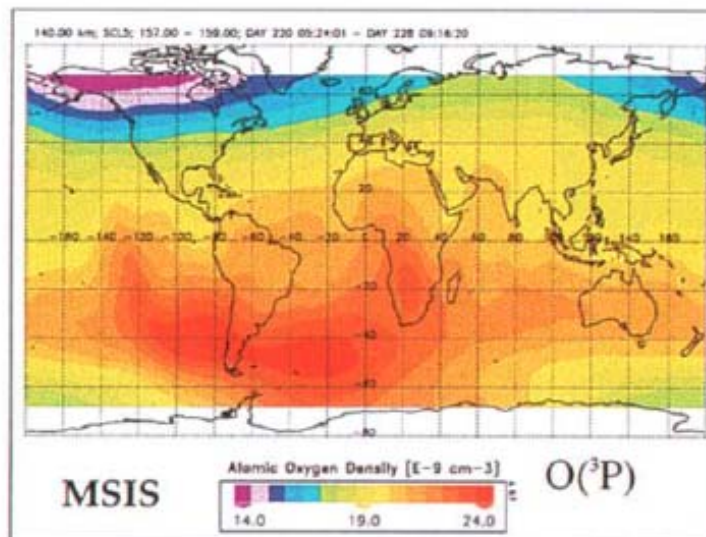
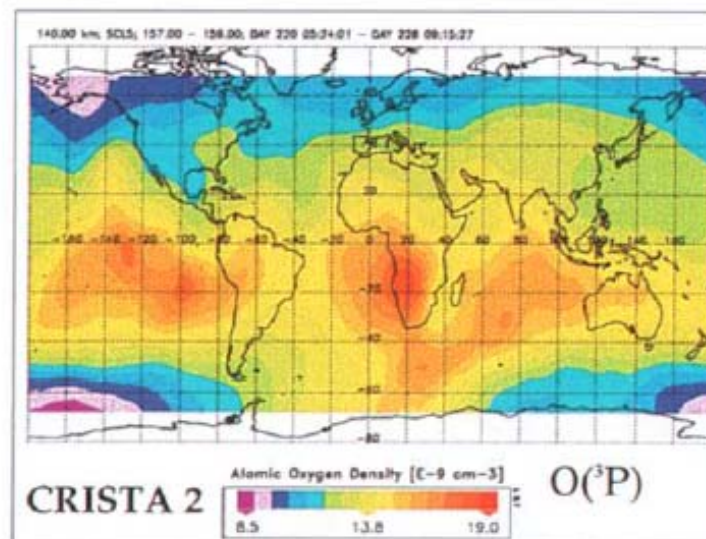


Plate 1. Atomic oxygen concentrations at 140 km measured by CRISTA-2 August 13 – 15, 1997 (upper panel). The color scale is $8.5 - 19.0 \cdot 10^9 \text{ cm}^{-3}$ in increments of $0.7 \cdot 10^9 \text{ cm}^{-3}$. MSIS model atomic oxygen concentrations (lower panel) calculated for the conditions of the experimental data. The color scale here is $14.0 - 24.0 \cdot 10^9 \text{ cm}^{-3}$ in increments of $0.7 \cdot 10^9 \text{ cm}^{-3}$.

Ionosphere-Thermosphere Validation Matrix

	T _n	U	V	O ₂	N ₂	O	NO	N	n _n (ρ)	n _e	O ⁺	NO ⁺	O ₂ ⁺	T _e	T _i	u _i	v _i
ISRs	x ¹	x ¹	x ¹							x				x	x	x	x
Digisondes										x						x	x
SuperDarn																x	x
Imagers					x ²	x ²				x ²							
Accelerometers [†]										x							
Satellite Drag [‡]										x							
DE 2 [‡]	x	x	x	x	x	x		x	x	x				x	x	x	x
AE [‡]				x	x	x	x	x	x	x	x	x	x	x	x	x	
GPS systems										x							
DMSP/NOAA										x				x	x	x ³	x ³
TIMED	x	x	x		x	x	x										
SNOE								x									
Ground FPI	x	x	x														
GroundImager																	
ArchivedRocket [†]	x	x	x		x	x		x	x								
CHAMP	x									x							
SWARM									x							x	
GAIA	x	x	x	x	x	x			x	x	x	△	△	△	△	x	x

(from Psnuux&wjjxjsyfytss& fyjwfq)

¹ Below ~130 km

² O/N₂ during the day, electron densities at night, also coupling parameters. Useful composition data could not be obtained from POLAR and IMAGE

[†] In situ or mainly in situ measurements, DE 2 and AE were multi-instrumented missions

[‡] Only some of these variables were available on any particular rocket flight. Generally sporadic.

³ Derived quantities with assumptions

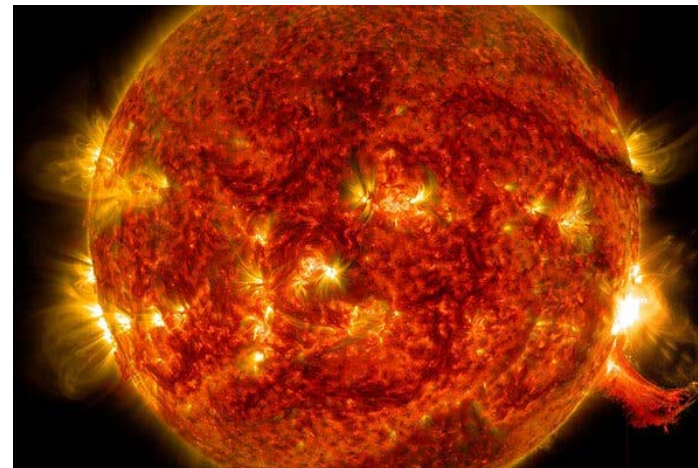
最近の話題より

2022年2月のスター・リンク衛星の落下事故

<https://www.nytimes.com/2022/02/09/science/spacex-satellites-storm.html>

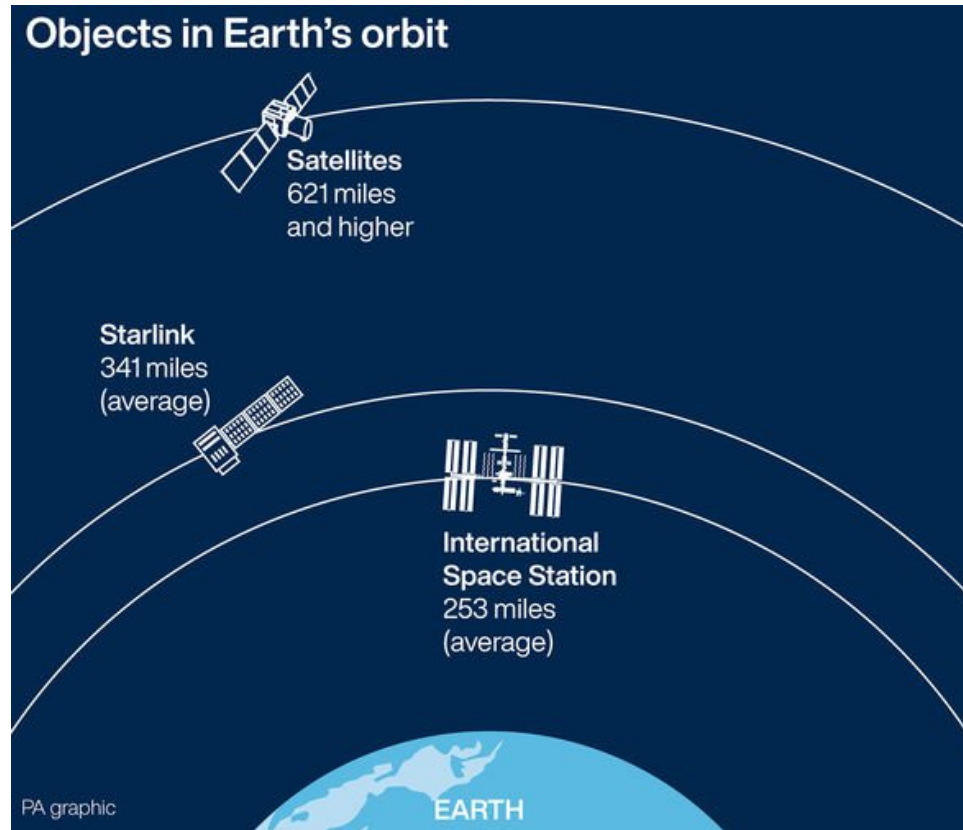
Solar Storm Destroys 40 New SpaceX Satellites in Orbit

The geomagnetic incident resulted in the Starlink transmitters drifting back into Earth's atmosphere, where they will burn up, potentially costing the company about \$100 million.



A geomagnetic storm triggered by a recent outburst of the sun knocked out up to 40 of 49 newly launched Starlink satellites.Credit...GSFC/NASA

<https://www.express.co.uk/news/science/1278064/Starlink-satellites-how-many-Starlink-satellites-has-SpaceX-launched>



Double minor geomagnetic storms heated the thermosphere.
Enhancements (>50 %) of the thermospheric mass density at 200 km caused a strong drag force to the starlink satellites.

Derivation of the thermospheric density from the satellite motion

Simplified theory

Air drag force

$$F_D = \frac{1}{2} \rho C_D (V_s - U)^2 A_r$$

ρ : atmospheric density
 C_D : drag coefficient (~2.2)
 V_s : velocity of the satellite
 U : wind velocity
 A_r : satellite cross-section

Energy of the artificial satellite (assuming circular motion)

$$E = \frac{1}{2} m V_s^2 - \frac{GMm}{r}$$

From a balance between gravitational and centrifugal forces, E can be written as

$$E = -\frac{GMm}{2r}$$

m : mass of the satellite
 G : universal gravitational constant
 M : mass of the Earth
 m : mass of the satellite
 r : distance between the center of the Earth and the satellite

Energy reduction rate caused by the air drag force

$$\frac{dE}{dt} = -F_D(V_s - U) = -\frac{1}{2} \rho C_D (V_s - U)^3 A_r$$

We assume $V = V_s - U \sim V_s$.

$$\frac{dE}{dt} = \frac{GMm}{2r^2} \frac{dr}{dt} = -\frac{1}{2} \rho C_D V^3 A_r$$

$$V = \sqrt{\frac{GM}{r}}$$

The rate of orbital decay or the atmospheric density is written as follows,

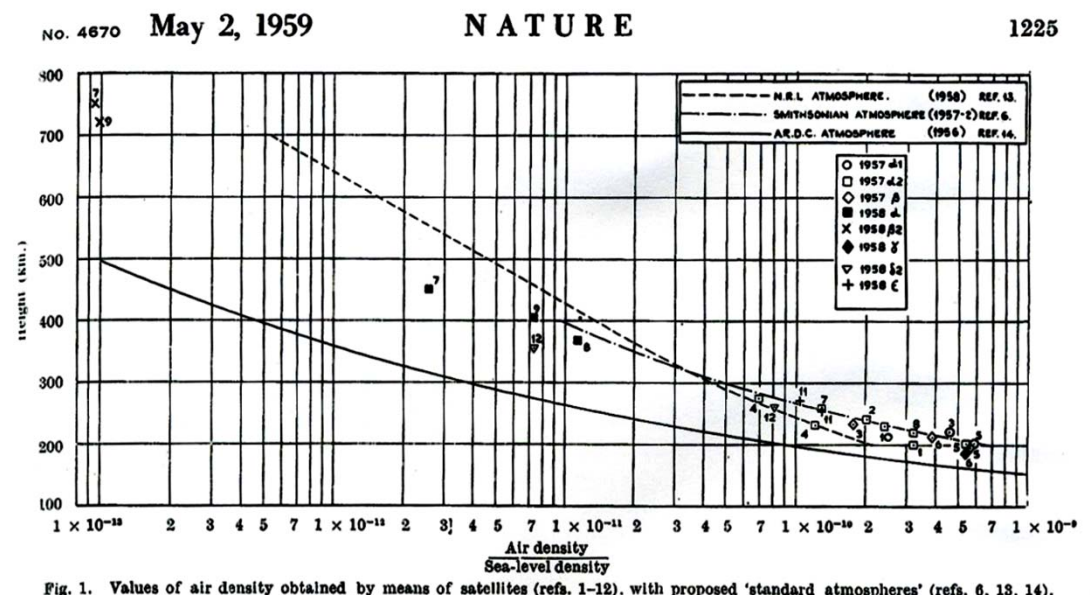
$$\frac{dr}{dt} = -\frac{\rho V C_D A_r r}{m} \quad \leftrightarrow \quad \rho = -\frac{m}{V C_D A_r r} \frac{dr}{dt}$$

Changes in the orbital period was used for estimation of the averaged atmospheric density in earlier times.

$$\dot{T} = \frac{dT}{dt} = -\frac{3\pi C_D A_r r}{m} \rho$$

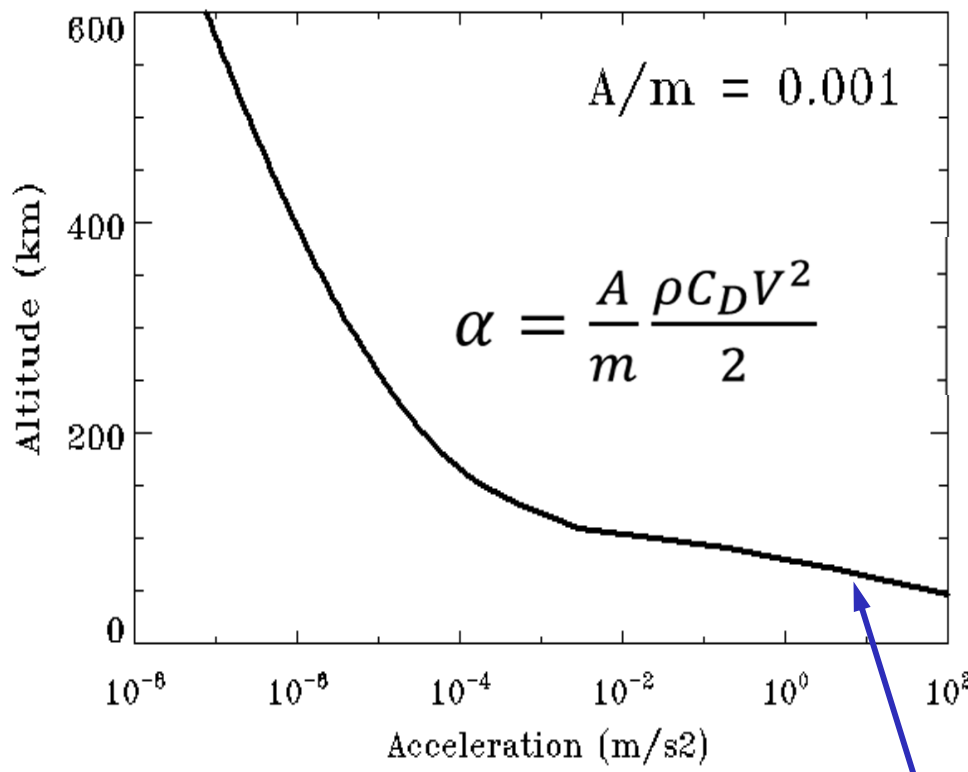
$$\left(T = \frac{2\pi r}{V} \right)$$

King-Hele [1959]

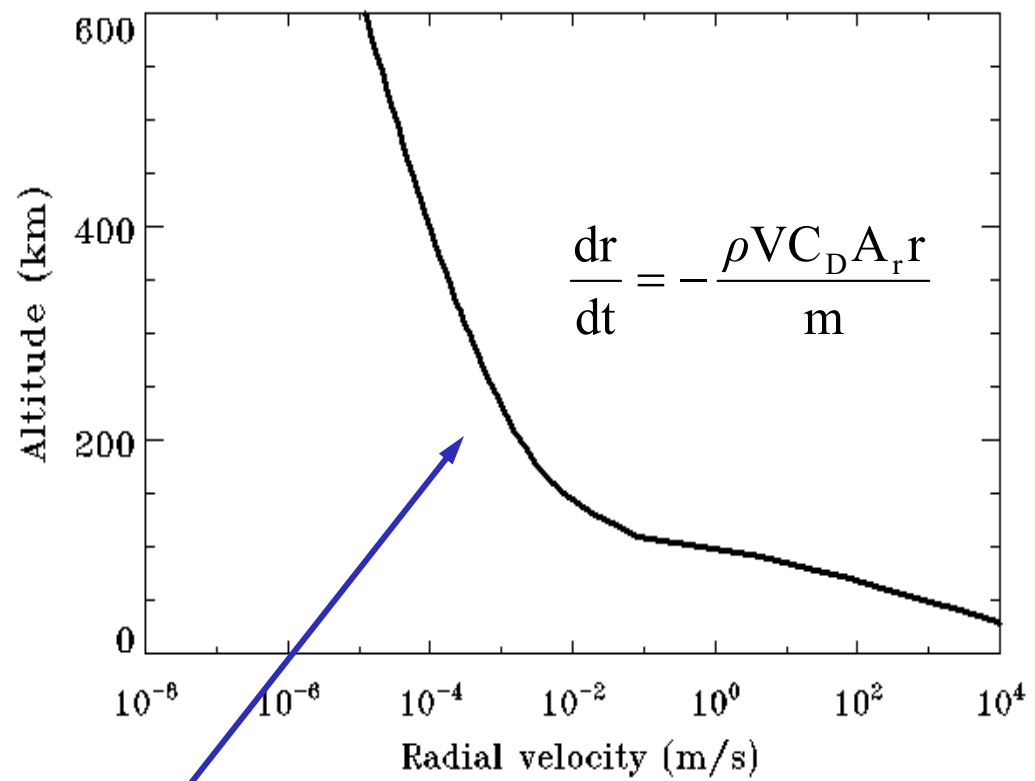


Example of calculations: satellite

Acceleration of satellite due to air drag force



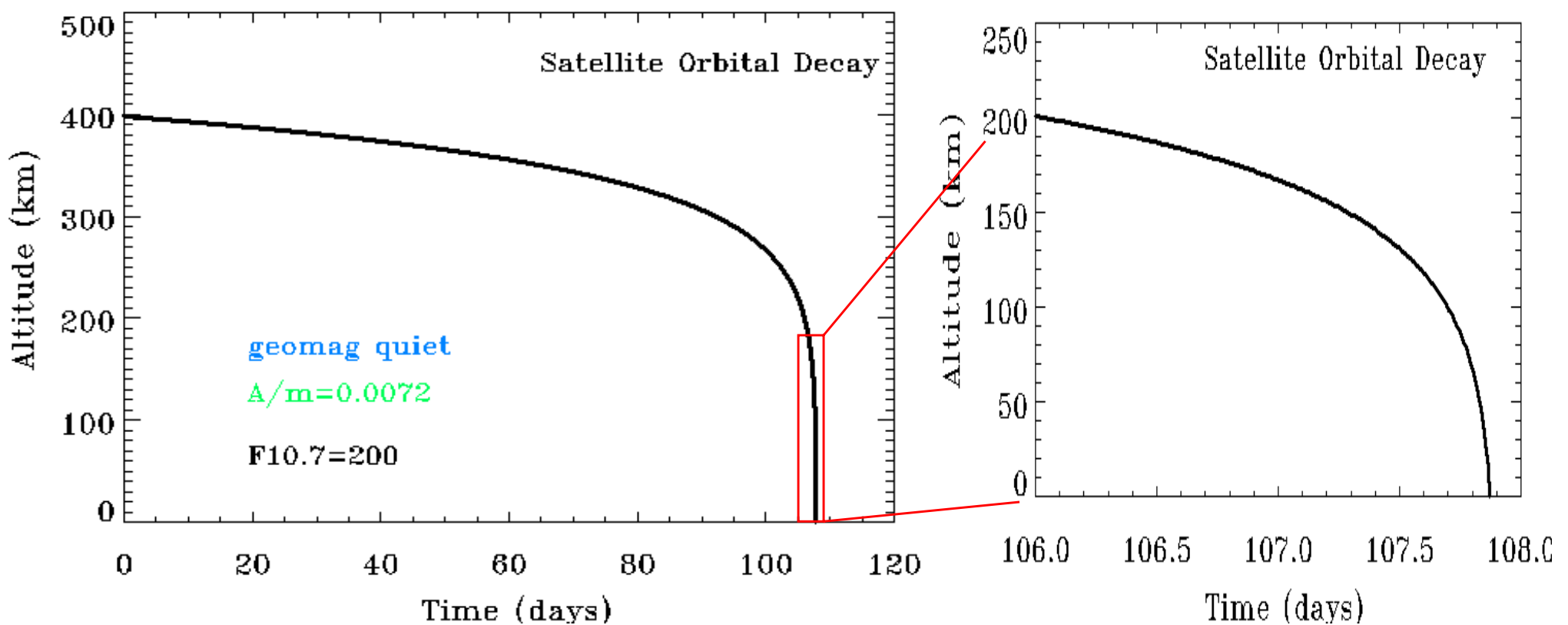
infall velocity (rate of fall) of satellite due to air drag force



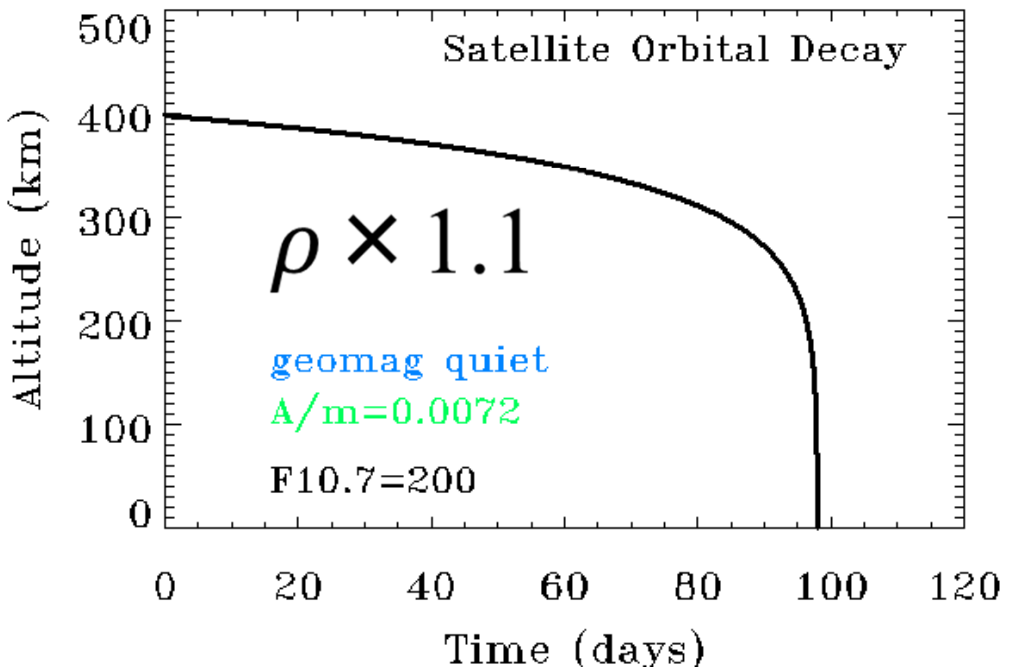
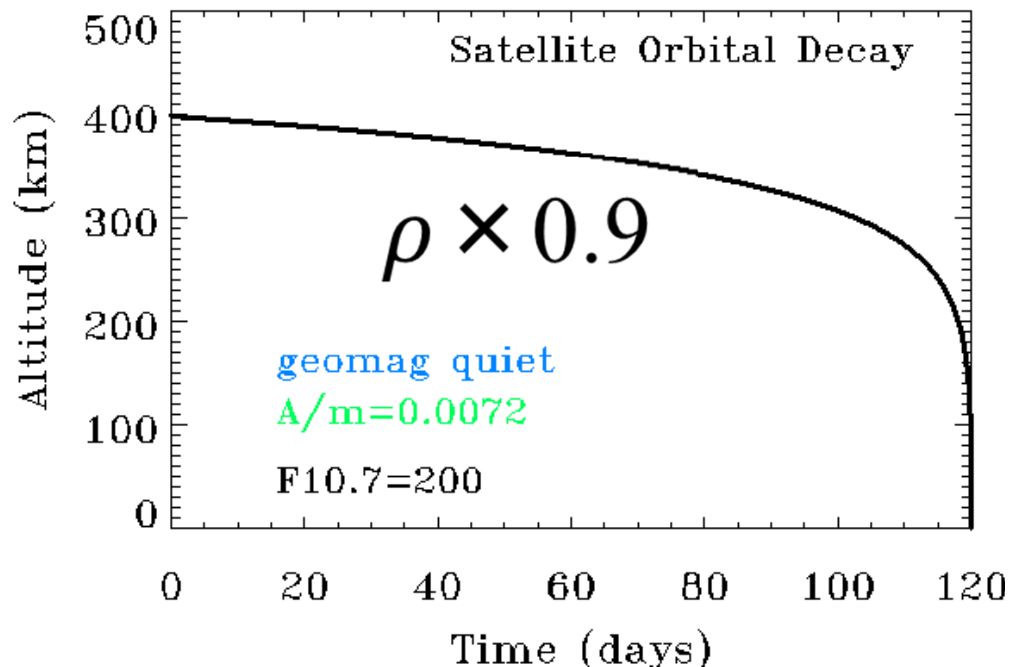
Shapes of the curve are strongly dependent on the thermospheric mass density.

Satellite mass (kg): 86
 Satellite area (m^2): 0.62
 Starting height (km): 400
 Solar Radio Flux (F10.7 index): 200
 Geomagnetic activity (Ap): 5 (quiet)

TAIYO satellite (Kato et al., 1979)



Lifetime of satellite at 200 km is $1 \sim 2$ days.

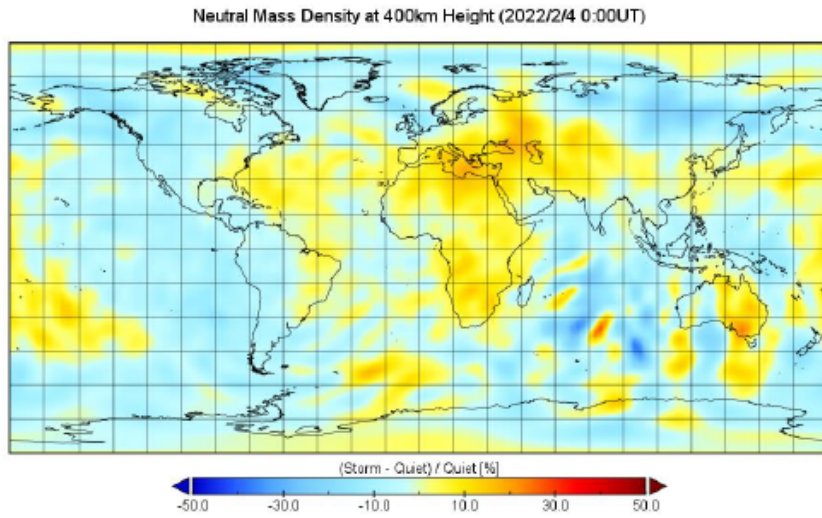


These simple calculations suggest that prediction of lifetime of the LEO satellite is quite difficult.

Kataoka et al. (Journal of Space Weather and Space Climate, 2022)

Unexpected space weather causing the reentry of 38 Starlink satellites in February 2022

400 km
Feb 4
00:00 UT



400 km
Feb 4
21:00 UT

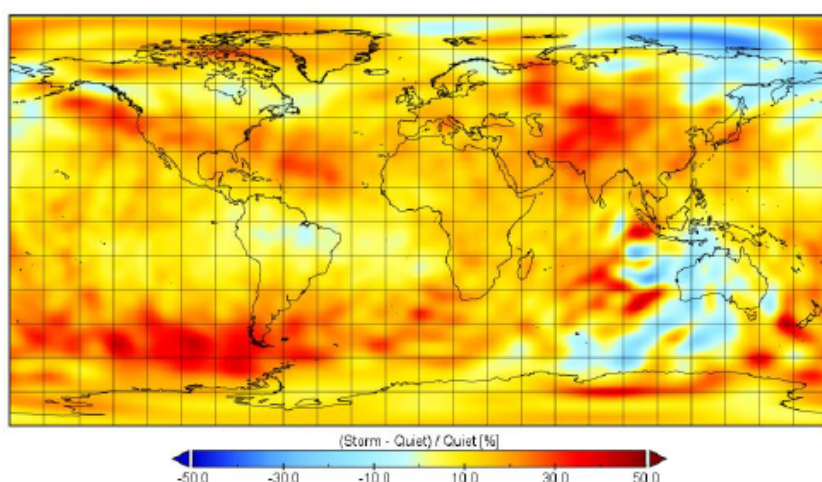


Figure 6. Simulation results of the thermospheric mass density at 400 km altitude, (storm-quiet)/quiet

Thermospheric mass density variations at about **400 km** during geomagnetically quiet (upper panel) and disturbed (lower panel) periods simulated with GAIA.

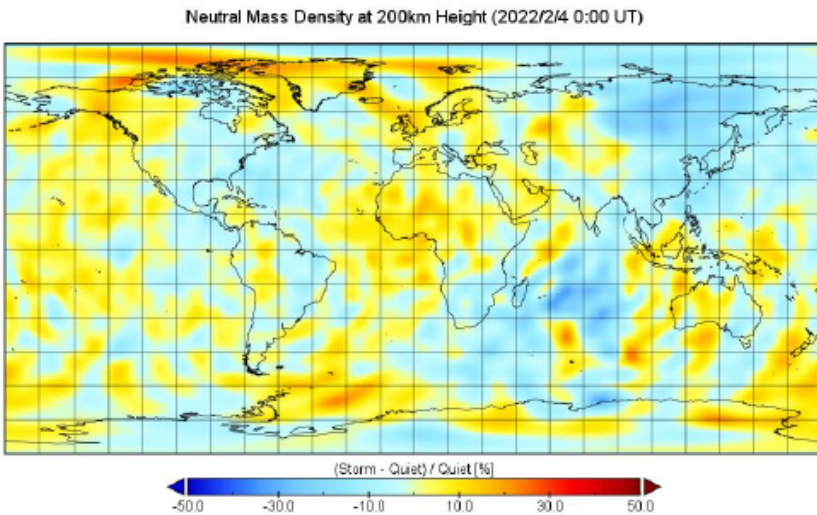
Kataoka et al. (2022)

GAIA simulations presented by NICT

R nsnkyw%tkA%yjwsf@Fkkfnw%fsi%
Htr r zsmhfyt sx%r fyjwfqx%is%ufufsjaxj .
https://www.soumu.go.jp/main_content/000794766.pdf

Kataoka et al. (2022)

200 km
Feb 4
00:00 UT



200 km
Feb 4
00:00 UT

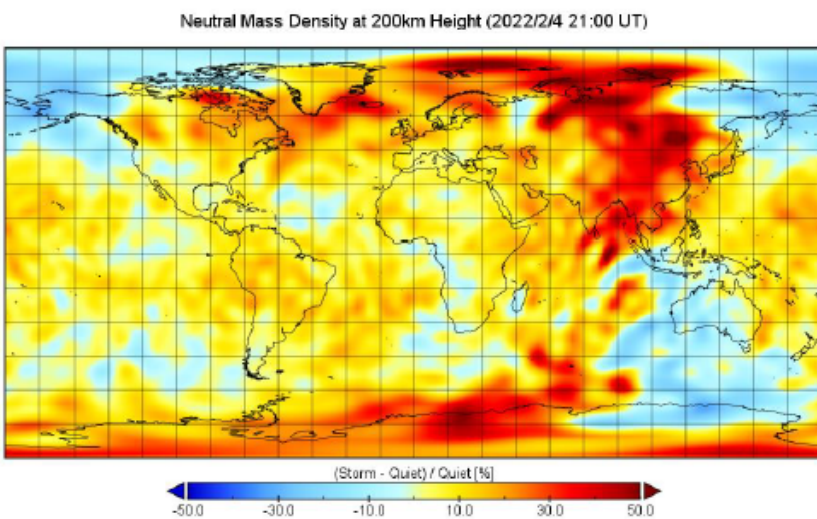


Figure 7. Simulation results of the thermospheric mass density at 200 km altitude, (storm-quiet)/quiet in %, for 0000 UT and 2100 UT on February 4, 2022. The selected quiet day is February 1, 2022.

Thermospheric mass density variations at about **200 km** during geomagnetically quiet (upper panel) and disturbed (lower panel) periods simulated with GAIA.

Simulation results suggest that the wave-like patterns are superimposed on the mass density enhancements ($> 50 \%$), which was likely caused by horizontal expansion of the heated air. Therefore, the actual thermospheric disturbances at around 200 km altitude might occur with larger amplitude in the wider area than those we thought in some cases.

SGEPSS将来構想

http://www.sgepss.org/sgepss/shorai/SGEPSS_syorai_digest_Jan2013.pdf

熱圏・電離圏が
大きく関わる部分：

安全な衛星運用
宇宙通信の維持

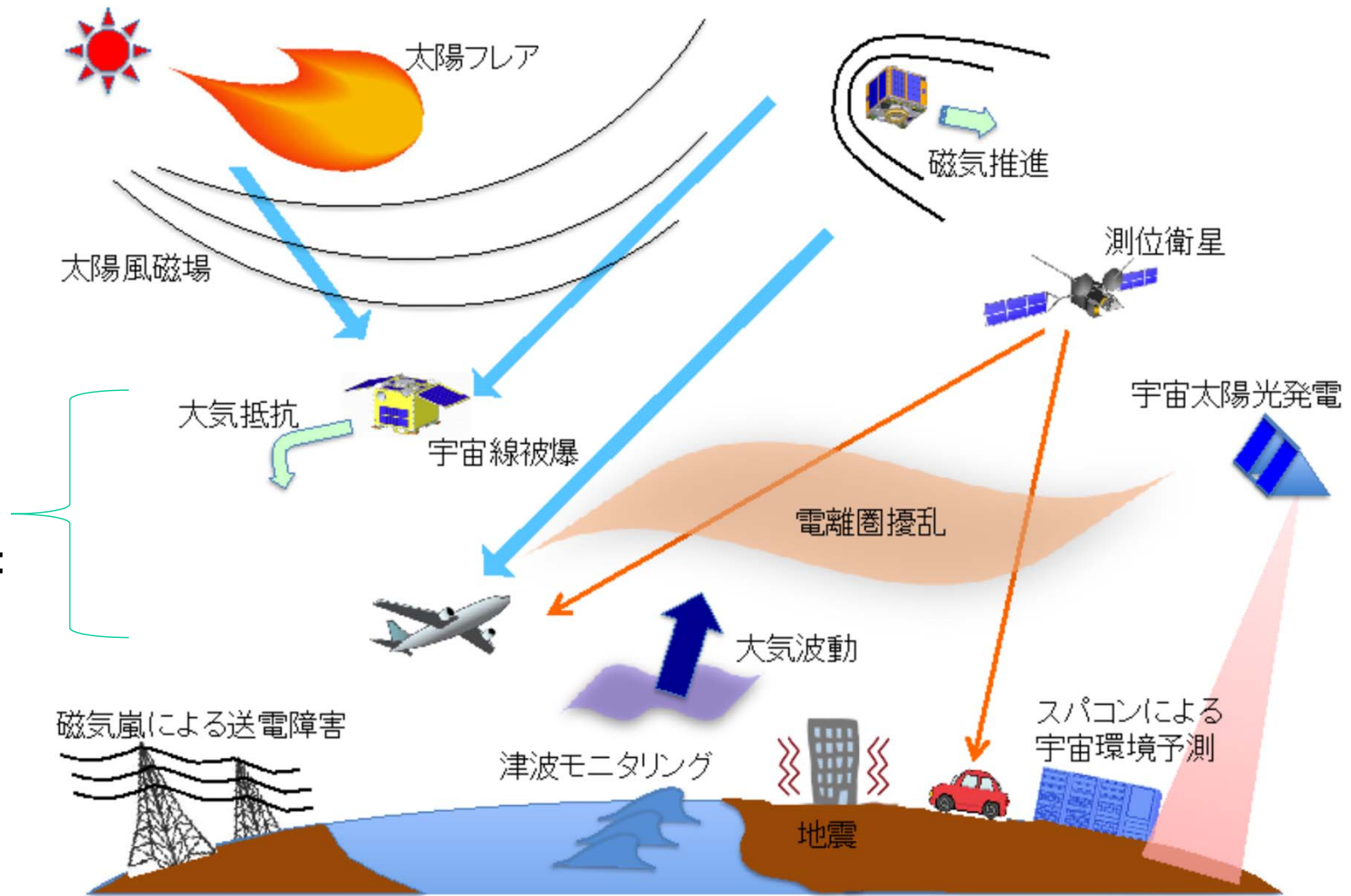


図 3.1 太陽地球圏と人間活動とのかかわり

まとめ

地上(レーダー、光学観測)・衛星観測、全球モデルの進展により、磁気嵐時の熱圏変動や、下層大気起源の熱圏変動が明らかになってきた。

特に、近年のCHAMPによる、熱圏大気質量密度計測は大きな進展であった。ただし、大気組成の時空間変動に関しては十分なデータがない。

さらに、高度150-250kmでの熱圏変動はよくは理解されていない(Space-Xの衛星事故はその表れ)。

今後の研究の方向性:ドラッグデータや、ありとあらゆるデータを使って、データ同化→予報研究、または機械学習による予報が進展するかもしれない。